HEALTH AND MEDICINE

Emergence of a senescent and inflammatory pulmonary CD4$^+$ T cell population prior to lung allograft failure

Sajad Moshkelgosha[1], Liran Levy[1,2], Shahideh Safavi[1,3], Sumiha Karunagaran[1], Gavin Wilson[1], Benjamin Renaud-Picard[1,4], Goodness Madu[1], Rashi Ramchandani[1], Jillian Oliver[1], Tatsuaki Watanabe[1,5], Ke Fan Bei[1], Betty Joe[1], Qixuan Li[6], Ella Huszti[6], May Cheung[1], David Hedley[7], Jonathan Yeung[1,8,9], Shaf Keshavjee[1,8,9], Tereza Martinu[1,8,10], Stephen Juvet[1,8,10]*

Survival after lung transplantation is limited by chronic lung allograft dysfunction (CLAD), an alloimmune fibrotic process leading to death or retransplantation after a median of 6 years. Immunosuppression fails to prevent CLAD, suggesting the existence of drug-resistant alloimmune pathways. We used time-of-flight mass cytometry to identify cells enriched in the bronchoalveolar lavage of patients with subsequent acute lung allograft dysfunction (ALAD), a risk factor for CLAD. We show that CD4$^+$CD57$^+$PD1$^+$ T cells emerge in stable patients, conferring risks for ALAD, CLAD, and death. These cells are senescent, secrete inflammatory cytokines, and fall into two oligoclonal subsets with putative cytotoxic and follicular helper functions. Last, they are associated with fibrosis in mouse and human lung allografts, where they localize near airway epithelium and B cells. Together, our findings reveal an inflammatory T cell population that predicts future lung allograft dysfunction and may represent a rational therapeutic target.

INTRODUCTION

The study of allograft rejection has led to important advances in our understanding of cellular immunity (*1*). Unfortunately, solid organ transplantation continues to be hampered by high rates of chronic rejection and graft failure despite the availability of potent immunosuppressive drugs. In lung transplantation (LT), which remains the only life-prolonging therapy for many cases of end-stage lung disease, median graft survival is only 6 years (*2*) due to chronic lung allograft dysfunction (CLAD). CLAD is the result of a progressive scarring process due to accumulated injuries resulting from alloreactivity and innate immune activation caused by donor brain death, ischemia-reperfusion injury, posttransplant infections, gastroesophageal reflux, and air pollution (*3*). Both acute T cell–mediated rejection and antibody-mediated rejection are well-recognized CLAD risk factors (*4*, *5*).

LT recipients often grapple with episodes of acute lung allograft dysfunction (ALAD) (*6*). We defined ALAD as a marked decrement in lung function—quantified by a decline in the forced expiratory volume in 1 s (FEV1) by 10% or more from its prior value. Despite exhaustive history, physical examination, and diagnostic testing including thoracic imaging and bronchoscopy, the cause of ALAD often is not definitively identified. Recurring ALAD events may be the result of rejection or uncontrolled alloimmunity that cannot be identified due to the poor diagnostic accuracy of transbronchial biopsies (*7*, *8*).

Bronchoalveolar lavage (BAL) is a technique in which saline instilled via a bronchoscope wedged in a pulmonary segmental airway is aspirated into a collection trap. BAL permits microbiologic and cytologic analysis of the distal lung compartments including the small airways and alveolar spaces. We have been studying cellular elements of the BAL using advanced multiparametric analytical approaches for the past several years (*6*, *9*–*12*). Using single-cell RNA sequencing (scRNA-seq), we recently identified specific alveolar macrophage populations associated with ALAD episodes and CLAD (*6*), which may represent both a mechanistic link between inflammatory insults such as infection and rejection, as well as a potential target for therapeutic intervention.

Prior studies by several groups have examined specific BAL T cell populations in LT recipients. An early work examined the question of whether changes in the CD4:CD8 ratio among BAL T cells might differentiate infection from rejection (*13*). Later studies examined whether T cell activation (*14*), differentiation (*15*), regulatory T cells (T_{regs}) (*16*), and apoptosis (*17*) could distinguish CLAD, acute rejection, and infection (*18*). High variability between LT recipients meant that such distinctions were difficult (*18*) and not useful in an individual patient. Moreover, because acute rejection and infection and CLAD can all coexist, and there are large overlaps in the distributions of prespecified BAL immune cell populations between these clinical entities, these hypothesis-directed analyses have not led to the identification of useful biomarkers or mechanistic insights.

Here, we used time-of-flight mass cytometry (CyTOF) (*19*), a high-dimensional technique in which the expression of up to 40 cell-associated proteins can be analyzed simultaneously, coupled with unbiased differential discovery approaches, to identify CD4$^+$CD57$^+$PD1$^+$ T cells as a predictor of incident ALAD and CLAD. Apart from their usefulness as a biomarker, our data implicate CD4$^+$CD57$^+$PD1$^+$ T cells

[1]Toronto General Hospital Research Institute, University Health Network, Toronto, ON, Canada. [2]Sheba Medical Center, Sackler School of Medicine, Tel-Aviv University, Tel-Aviv, Israel. [3]Barts Health NHS Trust, London, UK. [4]Nouvel Hôpital Civil, Strasbourg, France. [5]Department of Thoracic Surgery, Institute of Development, Aging and Cancer, Tohoku University, Sendai, Japan. [6]Biostatistics Department, University Health Network, Toronto, ON, Canada. [7]Division of Medical Oncology, Department of Medicine, University of Toronto, Toronto, ON, Canada. [8]Toronto Lung Transplant Program, Ajmera Transplant Centre, University Health Network, Toronto, ON, Canada. [9]Division of Thoracic Surgery, Department of Surgery, University of Toronto, Toronto, ON, Canada. [10]Division of Respirology, Department of Medicine, University of Toronto, Toronto, ON, Canada.
*Corresponding author. Email: stephen.juvet@uhn.ca

in the mechanism of allograft loss. We find the cells in chronically rejected human and mouse lung allografts, show that they are clonally expanded, express transcripts associated with cytotoxic and helper functions, and find that they secrete inflammatory cytokines. Furthermore, they are senescent, hypoproliferative, and resistant to cell death in vitro. Our observations therefore suggest the existence of a specific alloimmune pathway that can escape conventional immunosuppression that may represent a valuable therapeutic target.

RESULTS

Identification of a T cell subset associated with ALAD

Early detection of alloimmune responses in the graft, before ALAD onset, is likely to provide both important prognostic information and an opportunity for early intervention. In pursuit of a greater understanding of ALAD mechanisms, we prospectively collected and viably cryopreserved BAL cells from 50 Toronto Lung Transplant Program (TLTP) LT recipients presenting for surveillance bronchoscopy at 3 months posttransplant and obtained two more follow-up samples from each recipient to form a longitudinal cohort (Fig. 1A and fig. S1). To facilitate identification of cell populations associated with ALAD, we randomly divided the cohort into discovery and validation subsets ($n = 25$ each; Table 1). Longitudinal samples in the discovery group were then used to search for differences in the BAL cellular composition between stable patients and those experiencing ALAD within 90 days of each bronchoscopy. We performed CyTOF (*19*) on BAL cells using a panel of 36 heavy metal–conjugated antibodies (table S1). Unsupervised multidimensional clustering of BAL $CD3^+$ T cells from samples in the discovery cohort using FlowSOM (*20*) revealed 20 cell populations including T_{regs}, naïve, central, and effector memory $CD4^+$ and $CD8^+$ T cells and gamma delta T cells (Fig. 1B). Relative expression of proteins associated with each of the 20 T cell populations is depicted in Fig. 1C. BAL T cells exhibited substantial inter- and intrapatient heterogeneity (fig. S2).

We used cluster identification, characterization, and regression [CITRUS (*21*)] on all BAL T cells from all the time points for all patients in the discovery cohort (fig. S3A). This analysis revealed that a $CD4^+CD57^+PD1^+$ T cell population and a $CD8^+CD57^+CD69^+$ T cell population were differentially represented between patients with and without ALAD within 90 days of at least one bronchoscopy (fig. S3, B and C). To account for the paired design of our cohort (multiple samples per patient) and for longitudinal sampling over time, we also applied a generalized linear mixed model (GLMM) pipeline described for CyTOF analysis (*22*). T cell subsets with greater representation in samples associated with ALAD compared to samples associated with stability were identified using this approach (Fig. 1D). Using the GLMM approach, we found that $CD4^+$ $CD57^+PD1^+$ T cells were the most significantly differentially represented T cell population in ALAD (Fig. 1, D and E; protein expression profiles of the other 20 T cell populations are shown in fig. S4). Two additional T cell populations were also significantly differentially represented in the GLMM analysis: $CD4^+CD161^+HLA\text{-}DR^+$ T cells, which were associated with stability rather than ALAD, and, as we saw using CITRUS, $CD8^+CD57^+CD69^+$ T cells (Fig. 1D). Collectively, these data suggested that there is a strong association between $CD4^+CD57^+PD1^+$ T cells and incident ALAD.

$CD4^+CD57^+PD1^+$ T cells appear in the BAL prior to the onset of acute and CLAD and are associated with increased mortality risk

Next, we assessed the relationship of BAL $CD4^+CD57^+PD1^+$ T cells to ALAD onset. We observed that, although patients with stable lung allograft function had low frequencies of $CD57^+PD1^+$ cells in the BAL $CD4^+$ T cell compartment (Fig. 2A), these cells typically accumulated in higher frequencies prior to the onset of ALAD (Fig. 2B). Receiver operating characteristic (ROC) curve analysis showed that having ≥7.8% of $CD57^+PD1^+$ cells in the BAL $CD4^+$ T cell compartment optimally discriminated patients with ALAD within 90 days from stable patients, with an area under the ROC curve of 0.76 (Fig. 2C). Using this criterion, 10 of 11 (91%) LT recipients with ALAD within 90 days of any of their bronchoscopies demonstrated ≥7.8% of $CD57^+PD1^+$ in the $CD4^+$ T cell compartment of at least one of their BAL samples; in contrast, only 3 of 14 (21%) stable LT recipients had $CD57^+PD1^+$ cells exceeding this threshold (Fig. 2D). Moreover, having this biomarker conferred a reduced time-to-ALAD in univariable survival analysis (Fig. 2E). We then applied the 7.8% threshold to the validation subset ($n = 25$) and observed a similar reduction in time-to-ALAD from the first appearance of the cells in LT recipients with at least one BAL sample in which it was exceeded, compared to LT recipients who did not have any BAL samples in which the threshold was exceeded (Fig. 2F). Together, these data illustrated that, in LT recipients developing subsequent allograft dysfunction, $CD57^+PD1^+$ cells frequently exceeded the 7.8% threshold in BAL samples obtained prior to ALAD and CLAD (fig. S5).

To examine whether the presence of $CD4^+CD57^+PD1^+$ T cells in the BAL samples of LT recipients increases the risk for CLAD, we followed all 50 individuals in our cohort for up to 2000 days post-LT (median follow-up 1788 days). Using the appearance of ≥7.8% of $CD57^+PD1^+$ cells in the BAL $CD4^+$ T cell compartment or the last analyzed BAL as the index event, we found that time-to-CLAD was significantly shorter in those patients whose BAL samples exceeded the 7.8% threshold (log-rank $P = 0.0071$; fig. S6A). We then performed Cox proportional hazards analysis, excluding two patients who developed CLAD prior to their final BAL samples (fig. S1). Treating the appearance of ≥7.8% of $CD57^+PD1^+$ cells in the BAL $CD4^+$ T cell compartment as a time-dependent covariate, Cox proportional hazards analysis revealed a hazard ratio (HR) of 3.61 [95% confidence interval (CI), 1.55 to 8.39] for time-to-CLAD. In this and other survival analyses, patients were followed until 31 December 2022 (median follow-up time from transplantation: 2245 days). The increased risk for CLAD associated with $CD4^+CD57^+PD1^+$ cells persisted in bivariable models adjusted for age at transplant (HR, 3.67; 95% CI, 1.57 to 8.55), recipient sex (HR, 3.45; 95% CI, 1.47 to 8.07), and primary cytomegalovirus (CMV) mismatch (donor seropositive and recipient seronegative; HR, 4.02; 95% CI, 1.70 to 9.52).

Similarly, a Cox proportional hazards model revealed that the appearance of ≥7.8% of $CD57^+PD1^+$ cells in the BAL $CD4^+$ T cell compartment was associated with an HR of 4.82 (95% CI, 1.8 to 13.1) for time-to-death or retransplantation. The effect persisted in bivariable models adjusting for age at transplant (HR, 4.82; 95% CI, 1.8 to 13.1), recipient sex (HR, 4.84; 95% CI, 1.8 to 13.2), and primary CMV mismatch (HR, 4.92; 95% CI, 1.8 to 13.4). These time-to-CLAD and time-to-death or retransplantation analyses are presented in table S4. We then examined time-to-death or retransplantation in a

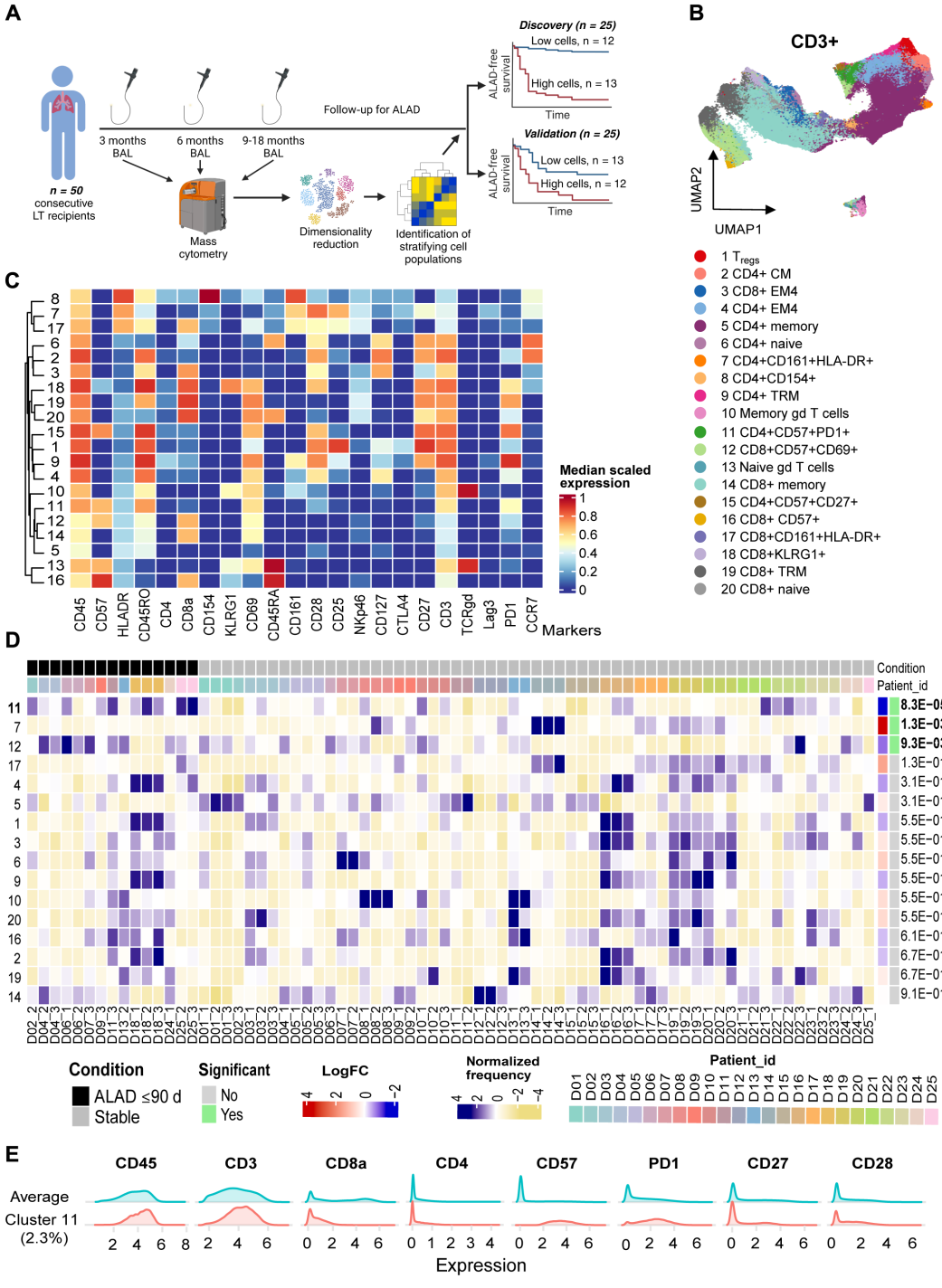

Fig. 1. Identification of a BAL CD3$^+$ T cell population associated with lung allograft dysfunction. (**A**) Study schematic. Fifty consecutive patients presenting for bronchoscopy at 3 months posttransplant were enrolled. For each enrolled patient, BAL cells at three time points (3, 6, and 9 months or next available) were collected. BAL cells were cryopreserved and subjected to CyTOF (see table S1); all samples from each patient were analyzed in the same CyTOF experiment. Patients were randomly divided into discovery ($n = 25$) and validation ($n = 25$) subsets (Table 1) to enable evaluation of differentially represented cell populations. (**B**) Uniform manifold approximation and projection (UMAP) plot of BAL CD3$^+$ cells falling into 20 clusters (highlighted in different colors) identified by FlowSOM. Annotation of cell populations is shown below the UMAP. (**C**) Heatmap depicting relative expression of 22 T cell–associated proteins across the 20 T cell populations in the discovery cohort. (**D**) Differential analysis heatmap of arcsine square root transformed cell frequencies that were subsequently normalized per cluster (rows; numbers along left side correspond to cell populations annotated in (B). Each column represents one BAL sample from the discovery cohort and is annotated along the bottom of the plot (patients D01 to D025, with the number following the underscore representing the specific BAL sample shown in that column). Statistically significant clusters are highlighted by green boxes at the right along with *P* values. d, days. (**E**) Analysis of molecules expressed by all cells (average) compared with those expressed by the most differentially represented cell population in patients with ALAD (cluster 11) reveals that the latter is CD45$^+$CD3$^+$CD4$^+$CD57$^+$PD1$^+$.

Table 1. Clinical characteristics of participants. Patients were randomized into a discovery group ($n = 25$) and a validation group ($n = 25$). LT, lung transplant; CMV, cytomegalovirus; D, donor; R, recipient. Comparisons between groups were made using Mann-Whitney *U* tests or Fisher's exact test, as appropriate.

	Discovery ($n = 25$)	Validation ($n = 25$)	*P* value
Recipient age at LT, years (means ± SD)	56 ± 14	56 ± 12	0.70
Donor age, years (means ± SD)	49 ± 14	51 ± 16	0.55
Donor type			
Donation after circulatory death, *n*	2	5	0.41
Donation after neurological death, *n*	23	20	
Cold ischemic time, min (means ± SD)	488 ± 153*	486 ± 166	0.71
Ex vivo lung perfusion, *n*	5	6	>0.99
Male recipient sex, *n*	17	19	0.75
Male donor sex, *n*	15	16	>0.99
Donor-recipient sex mismatch, *n*	2	4	0.67
Type of LT (bilateral LT, *n*)	19	19	1.0
Native lung disease			0.64
Interstitial lung disease, *n*	12	15	
Chronic obstructive pulmonary disease, *n*	9	6	
Other, *n*	4†	4‡	
CMV serology			>0.99
D+/R-, *n*	8	7	
D+/R+, D−/R+, D−/R−, *n*	17	18	

*$n = 2$ had missing data. †Cystic fibrosis ($n = 4$). ‡Cystic fibrosis ($n = 2$), graft-versus-host disease ($n = 1$), and pulmonary arterial hypertension ($n = 1$).

survival analysis landmarked at 12 months posttransplant. LT recipients with ≥7.8% of $CD57^+PD1^+$ cells in the BAL $CD4^+$ T cell compartment had an increased risk of death or retransplantation ($P = 0.00079$; Fig. 2G).

The use of ex vivo lung perfusion (EVLP) to evaluate donor lung grafts has increased the donor pool by enabling a careful functional evaluation of the graft prior to transplant (*23*). Some preclinical data suggest that EVLP may inhibit alloimmune priming by removing donor antigen-presenting cells (*24*), although an impact of EVLP on rejection and CLAD has not been demonstrated (*25*). In agreement with these findings, receipt of lungs evaluated on EVLP was not associated with a reduced likelihood of $CD4^+CD57^+PD1^+$ T cells appearing in posttransplant BAL (fig. S6B).

Anti-human leukocyte antigen donor-specific antibodies (DSAs) are an adverse prognostic factor in LT (*26*). Patients with ≥7.8% of $CD57^+PD1^+$ cells in the BAL $CD4^+$ T cell compartment were not more likely to develop de novo DSAs than those without (Fig. 2H). Similarly, BAL $CD4^+CD57^+PD1^+$ T cells were not simply a surrogate for other conventional clinical and bronchoscopic parameters because clinical symptoms, biopsy-proven vascular or airway rejection, BAL pathogens, and antimicrobial treatments did not differ significantly between patients with and without ≥7.8% of $CD57^+PD1^+$ cells in the BAL $CD4^+$ T cell compartment (table S2). Furthermore, although the number of events was small, having $CD57^+PD1^+$ cells above the 7.8% threshold was not clearly associated with an immediate postbronchoscopy augmentation of immunosuppression or change in calcineurin inhibitor (table S3).

Together, these observations indicate that BAL $CD4^+CD57^+PD1^+$ T cells may be a useful biomarker of incident lung allograft dysfunction that adds significant diagnostic utility to conventional clinical monitoring.

$CD4^+CD57^+PD1^+$ T cells are present in chronically rejected human lung allografts

These observations suggested that $CD4^+CD57^+PD1^+$ T cells might lie on the mechanistic pathway leading to lung allograft fibrosis. Therefore, we sought to identify them in CLAD lung tissue obtained at the time of retransplantation (*27*) using imaging mass cytometry [IMC (*28*)] (Fig. 3A). We have previously published IMC analysis focusing on a broad description of the epithelial and immune cell populations identifiable in CLAD lungs (*29*). Here, we used this dataset to investigate the spatial distribution and cellular interactions of $CD4^+CD57^+PD1^+$ T cells. CLAD ($n = 8$) and normal lung tissue sections obtained from organ donors ($n = 2$) or lung cancer lobectomies (taken from a region away from the tumor; $n = 2$) were stained with a panel of 35 heavy metal–conjugated antibodies (table S5) and subjected to IMC. Unsupervised clustering performed on all samples using Histocat (*30*) identified multiple myeloid, epithelial, and T cell populations, including $CD4^+CD57^+PD1^+$ T cells as one of the cell populations present (cluster 50 in Fig. 3B). In reconstructed images, $CD4^+CD57^+PD1^+$ T cells were visible in both control and CLAD lung tissue (Fig. 3C). There was a nonstatistically significantly higher number of $CD4^+CD57^+PD1^+$ T cells in CLAD lung tissue compared to control lung tissue (Fig. 3D); the difference appeared to be driven by two CLAD lungs with higher frequencies

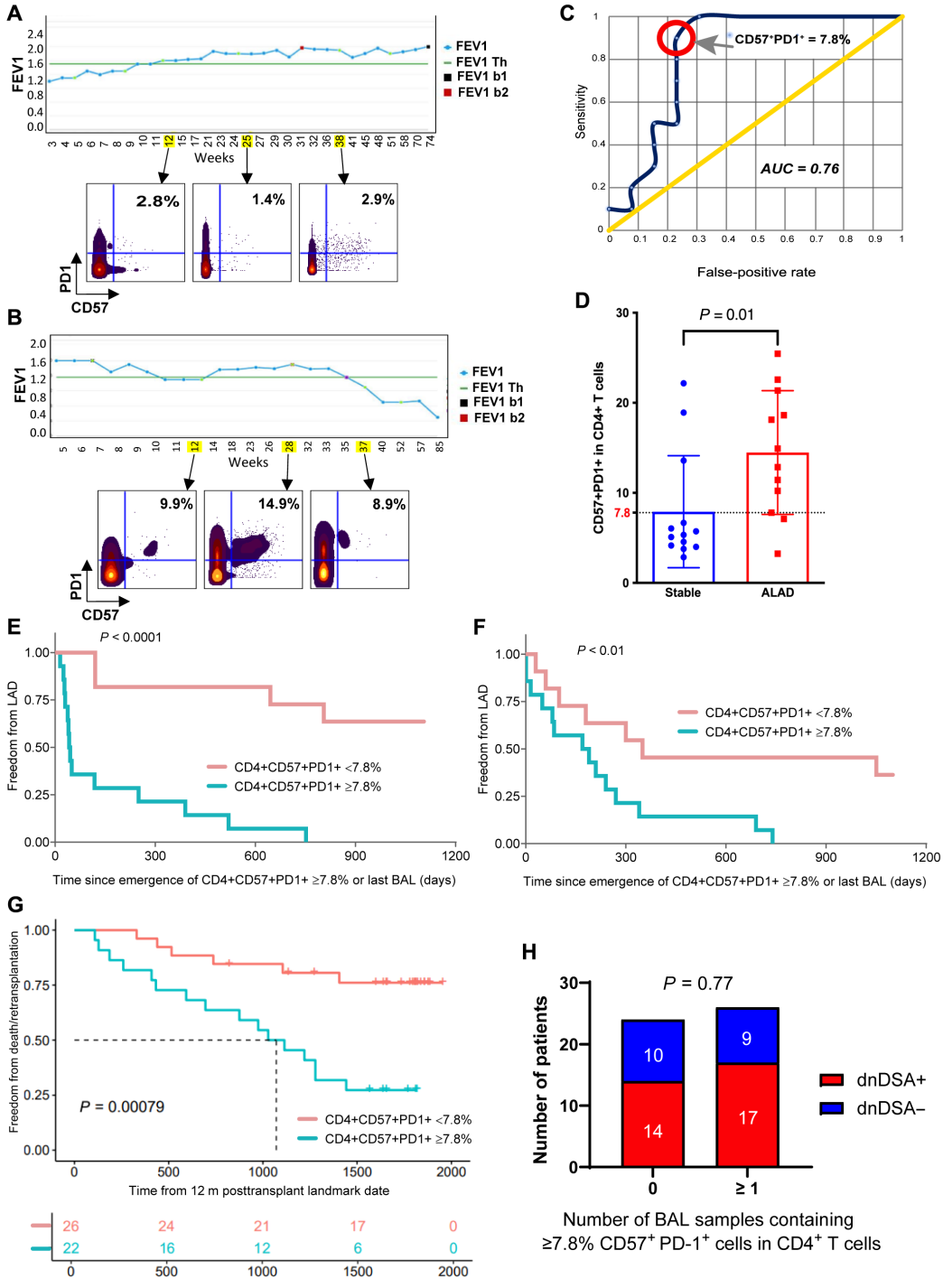

Fig. 2. BAL $CD4^+CD57^+PD1^+$ T cells confer risk for acute and CLAD and death/retransplantation. Examples of FEV1 over time in stable (**A**) and ALAD (**B**) discovery cohort patients. Blue, FEV1 trend line; red and black, highest achieved FEV1 values (FEV1 b1 and FEV1 b2); green, threshold (FEV1 Th) of 80% of average of FEV1 b1 and b2, below which CLAD is diagnosed if dysfunction persists for ≥3 months (*69*); yellow, BAL dates; CD4 versus CD57 scatterplots ($CD4^+$ gate) are shown. (**C**) ROC curve analysis of $\%CD57^+PD1^+$ cells in BAL $CD4^+$ T cells for subsequent diagnosis of ALAD. AUC = 0.76. Circle, $\%CD57^+PD1^+$ optimally discriminating patients with ALAD/stable patients (7.8%). (**D**) Highest $\%CD57^+PD1^+$ in all samples from each patient (discovery cohort, $n = 25$), stratified by the presence/absence of ALAD within 90 days. Mann-Whitney, $P = 0.0018$. (**E**) Time–to–lung allograft dysfunction from ≥7.8% of $CD57^+PD1^+$ cells in BAL $CD4^+$ T cells (blue line) or from final BAL (red line) in discovery cohort ($n = 25$). Log-rank $P < 0.0001$. (**F**) Time–to–lung allograft dysfunction from ≥7.8% of $CD57^+PD1^+$ cells in BAL $CD4^+$ T cells (blue line) or from final BAL (red line) in the validation cohort ($n = 25$). Log-rank $P < 0.02$. (**G**) Time-to-death or retransplantation from 12 months (m) posttransplant for the entire cohort, stratified by whether $CD57^+PD1^+$ T cells ever (blue line) or never (red line) accounted for ≥7.8% of the $CD4^+$ compartment. Log-rank, $P = 0.00079$. (**H**) Of the 31 patients developing de novo DSAs, 17 (54.8%) had ≥7.8% of $CD57^+PD1^+$ in BAL $CD4^+$ T cells in ≥1 BAL sample; 9 of 19 (47.3%) not developing de novo DSAs had $CD57^+PD1^+$ cells ≥7.8% of $CD4^+$ T cells in ≥1 BAL sample. Fisher's exact test, $P = 0.77$.

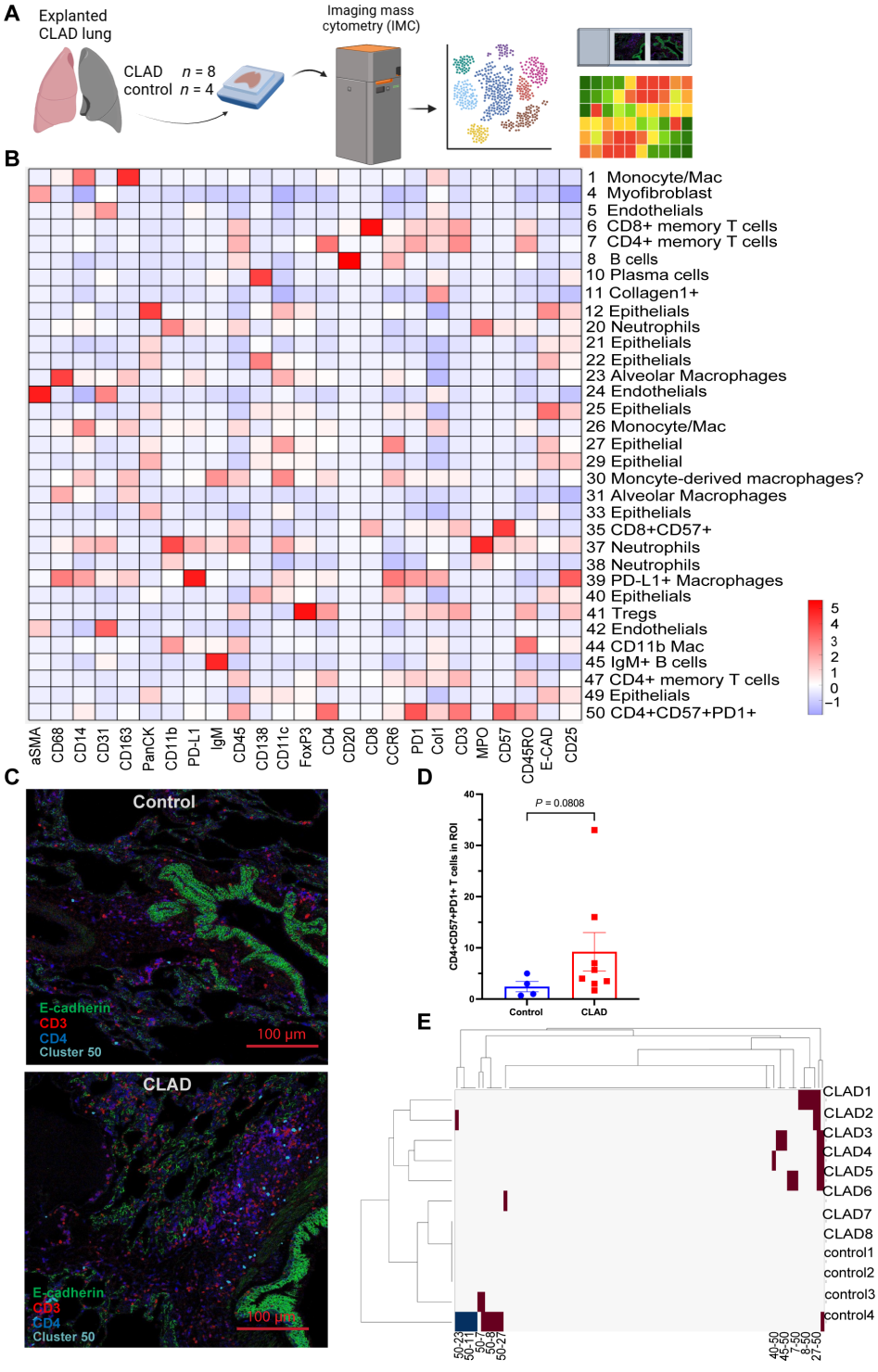

Fig. 3. CD4$^+$CD57$^+$PD1$^+$ T cells are found in CLAD lung tissue. (**A**) Analysis workflow. (**B**) Heatmap of protein expression (*x* axis) by selected cell clusters identified in IMC (annotated along the right side). Red color indicates higher expression levels. Cluster 50 represents CD4$^+$CD57$^+$PD1$^+$ T cells. (**C**) Reconstructed IMC images of CLAD lung tissue obtained at the time of retransplantation (top) and normal donor lung tissue (bottom). E-cadherin$^+$ epithelial cells (green pseudocolor), CD3$^+$ T cells (red pseudocolor), CD4$^+$ cells (blue pseudocolor), and CD4$^+$CD57$^+$PD1$^+$ T cells (cluster 50, pale blue pseudocolor) are shown. (**D**) Number of CD4$^+$CD57$^+$PD1$^+$ T cells per ROI in control and CLAD lungs. Mann-Whitney *U* test, $P = 0.0808$. Data from 3 ROIs from each of $n = 8$ CLAD, and $n = 4$ normal lungs are shown. (**E**) Neighborhood analysis of CD4$^+$CD57$^+$PD1$^+$T cells (cluster 50, shown in columns) in CLAD and control lungs (rows). Annotations along the *x* axis indicate interactions (e.g., 50-8 means an interaction between cluster 50 and cluster 8 from (B)] with either significant proximity (brown) or avoidance (blue).

of these cells (fig. S7). Neighborhood analysis (Fig. 3E) revealed that $CD4^+CD57^+PD1^+$ T cells were frequently located adjacent to trafficking B cells ($CD20^+CCR6^+$, cluster 8) and epithelial cells (cluster 27). Proximity to these other cell populations was more consistently observed in CLAD lungs compared to control lungs (Fig. 3E). The proximity of $CD4^+CD57^+PD1^+$ T cells to B cells and epithelial cells in CLAD lung tissue may indicate that they are involved in disease development.

$CD4^+CD57^+PD1^+$ T cells are associated with CLAD-like pathology in a mouse lung transplant model

Given our observations in human CLAD lung tissue, we asked whether the severity of allograft fibrosis might correlate with the infiltration of a similar T cell population in mice. We have developed a minor alloantigen-mismatched mouse orthotopic LT model in which a minimal graft storage period prior to transplantation results in mild or absent allograft fibrosis at 28 days posttransplant, whereas prolonged warm and cold ischemic storage prior to transplantation leads to B cell– and alloimmune-dependent fibrosis with features of human chronic lung allograft rejection (Fig. 4A) (*31*). Allografts were scored in blinded manner using our published scoring system (*32*), which includes assessment of the proportion of the allograft affected by interstitial inflammation and fibrosis. As we have observed previously (*31*, *32*), pathology was variable, with some animals exhibiting higher degrees of fibrosis and inflammation (Fig. 4, B and C). At 28 days after transplantation, lung allografts contained ~5 to 25% of $CD57^+PD1^+$ T cells in the $CD4^+$ compartment, whereas they were rare in normal mouse lungs (Fig. 4, D to F). Allografts with higher degrees of pathology, as determined by the presence of both interstitial inflammation and parenchymal fibrosis, had higher frequencies of $CD57^+PD1^+$ T cells compared to those with a low degree of pathology (Fig. 4F). Furthermore, $CD4^+CD57^+PD1^+$ T cells were readily detectable in allograft sections by immunofluorescence (Fig. 4G). Together, our findings indicate that $CD4^+CD57^+PD1^+$ T cells accumulate in mouse and human lung allografts during chronic rejection and that their abundance is correlated with the severity of fibrosis.

Identification of two transcriptionally distinct $CD4^+CD57^+PD1^+$ cell subsets using CITE-seq

To characterize gene expression in $CD4^+CD57^+PD1^+$ T cells, we enriched $CD3^+$ T cells from four ALAD BAL samples and performed cellular indexing by transcriptomes and epitopes [CITE-seq (*33*)] with 5′ end sequencing (Fig. 5A). We applied a panel of oligonucleotide-conjugated antibodies, including CD4, CD57, and PD1, to ALAD BAL samples containing at least 7.8% of $CD57^+PD1^+$ cells in the $CD4^+$ T cell compartment as determined by flow cytometry. The conjugated oligonucleotides or antibody-derived tags (ADTs) identified in CITE-seq allowed confident linkage of transcriptomes with protein expression.

A total of 18946 cells were sequenced from the four ALAD samples. $CD4^+$ T cells fell into nine subclusters in multidimensional space (Fig. 5B). We used scTx (*34*), which allows distinction between donor and recipient cells on the basis of single-nucleotide variations (SNVs), to infer that 99.00 ± 1.17% of BAL T cells in these samples were recipient derived (fig. S8), essentially excluding the possibility that $CD4^+CD57^+PD1^+$ T cells originated in substantial numbers from the donor.

On the basis of CD57 and PD1 protein expression, $CD4^+CD57^+PD1^+$ T cells assembled into two main areas, cluster 4 and the closely adjacent clusters 1 and 2 (Fig. 5B and fig. S9, A and B). We noted that CD27 gene and protein expression was enriched in cluster 4 compared to clusters 1 and 2 (Fig. 5C). The $CD27^-$ population had a gene expression profile similar to peripheral helper T (Tph) cells described in rheumatoid arthritis (*35*); differentially expressed genes in this population included *CXCL13*, *TOX*, interleukin-21 (*IL21*), *CD40L*, *TIGIT*, *ICOS*, and *TNFSRF18* (Fig. 5D and fig. S9C). These cells are characterized by the absence of the conventional follicular helper T cell markers CXCR5 and Bcl6 and by expression of the chemokine CXCL13 (*35*, *36*). Accumulating studies have shown that Tph cells are involved in various acute and chronic inflammatory diseases (*35*, *37*) and can promote B cell differentiation into plasmablasts through interactions involving IL-21 and SLAMF5 (*35*). Therefore, the Tph-like features of $CD27^-$ $CD4^+CD57^+PD1^+$ T cells, along with their proximity to B cells (Fig. 3E), suggest that they might have the ability to provide B cell help.

The $CD27^+$ population expresses several cytotoxicity-related transcripts including granzymes and *NKG7* (Fig. 5D) (*38*). It also expresses *CXCR6*, which has been associated with tissue-resident memory $CD8^+$ T cell localization to airways (*39*) and is in keeping with our observation of $CD4^+CD57^+PD1^+$ T cells in proximity to epithelial cells (Fig. 3E).

$CD4^+CD57^+PD1^+$ T cells had some features in keeping with tissue-resident memory T (Trm) cells (*40*), which have been identified in transplanted lungs previously (*41*). Clusters 1, 2, and 4 expressed CD69 protein but low levels of its transcript; cluster 2 expressed transcripts for *ITGA1*, encoding the integrin CD49a. On the other hand, most BAL $CD4^+$ T cells, not just those expressing CD57 and PD1, in our dataset expressed *ITGAE* and its encoded protein CD103, albeit at varying levels (fig. S10). Further investigation with additional samples will be required to confirm whether $CD4^+CD57^+PD1^+$ T cells or their $CD27^+$ and $CD27^-$ subsets can be classified confidently as Trm cells.

We next examined T cell receptor (TCR) complementarity-determining region 3 (CDR3) sequences in the CITE-seq data, which revealed that $CD57^+PD1^+CD27^-$ cells are clonally expanded to a greater extent than $CD57^+PD1^+CD27^+$ and other BAL $CD4^+$ T cells (Fig. 5E). This suggested that they had recently undergone antigen-driven expansion in the lung. Analysis of the top 20 expanded TCR clonotypes did not infer any known cognate antigen (fig. S11). Pseudotime trajectory analysis revealed that $CD57^+PD1^+CD27^-$ cells and their $CD27^+$ counterparts may share a common origin (Fig. 5F). Together, the TCR sequence data and pseudotime analysis suggested that BAL $CD4^+CD57^+PD1^+$ T cells either differentiate into Tph or cytotoxic effector cells. The former have undergone significant clonal expansion, whereas the latter have a distinct TCR repertoire and less clonal expansion, suggesting that they may be responding to different antigens in the lung microenvironment.

Last, both $CD27^-$ and $CD27^+$ subsets demonstrated expression of previously defined senescence and exhaustion transcripts including *TIGIT*, *KLRG1*, *LAG3*, *HAVCR2* (encoding TIM-3), and *EOMES*, which have been described under different acute and chronic inflammatory conditions (*42*–*44*). This observation is in keeping with reports that have described different senescent $CD57^+$ and/or $PD1^+$ T cell populations in other disease states (*45*, *46*). Together, these findings suggest that $CD4^+CD57^+PD1^+$ fall into at least two groups with distinct transcriptional profiles and TCR repertoires. Additional confirmation of these observations in studies with larger numbers of cells and patients will be required.

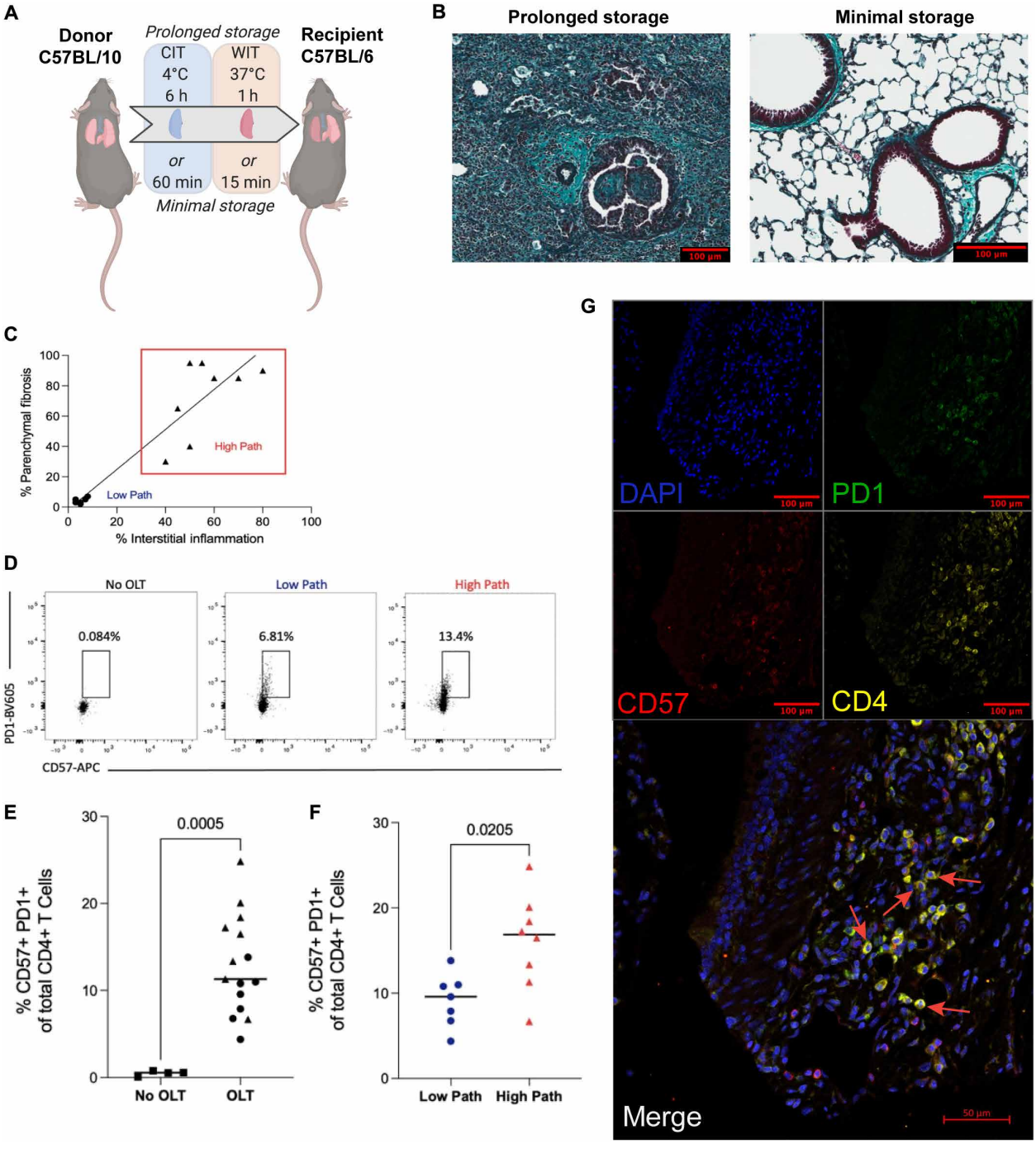

Fig. 4. CD4$^+$CD57$^+$PD1$^+$ T cells are associated with the degree of fibrosis in a mouse CLAD model. (**A**) C57BL/10 (B10) donor lungs underwent either prolonged [6-hour (h) cold ischemic time (CIT) at 4°C followed by 1-hour warm ischemic time (WIT) at 37°C] or minimal (60-min CIT followed by 15-min WIT) storage prior to orthotopic left lung transplantation (OLT) into minor alloantigen-mismatched C57BL/6 (B6) recipients. (**B**) Representative Masson trichrome–stained sections (collagen stains blue) of mouse lung allografts from prolonged (left) and minimal storage (right) grafts 28 days after LT. Graft histology was scored (*32*) to quantify the percentage of graft affected by interstitial inflammation and parenchymal fibrosis. Scale bars, 100 µm. (**C**) Fibrotic pathology was variable and fell into high (High Path, red box, triangles) and low (Low Path, circles) severity groups when plotted according to the percentage of graft affected by parenchymal fibrosis and interstitial inflammation. (**D**) Flow cytometry of digested mouse lung grafts showing CD4$^+$CD57$^+$PD1$^+$ T cells in Low and High Path groups (middle and right); these cells are absent from normal lungs (No OLT). In (**E**) and (**F**), High Path grafts are represented as triangles, and Low Path grafts are represented as circles. (E) Percentage of CD4$^+$ T cells expressing CD57 and PD1 in naïve B6 lungs (No OLT, squares), Low Path grafts (circles), and High Path grafts (triangles). Student's *t* test, $P = 0.0005$. (F) Percentage of CD4$^+$ T cells expressing CD57 and PD1 is shown for Low Path grafts (circles) and High Path grafts (triangles). Student's *t* test, $P = 0.0205$. (**G**) Immunofluorescence of prolonged storage. High Path lung allograft showing PD1 (green), CD57 (red), CD4 (yellow), and DAPI (blue) and merged image. Red arrows indicate examples of cells expressing all three markers. Scale bars, 100 µm (single color images) and 50 µm (merged image).

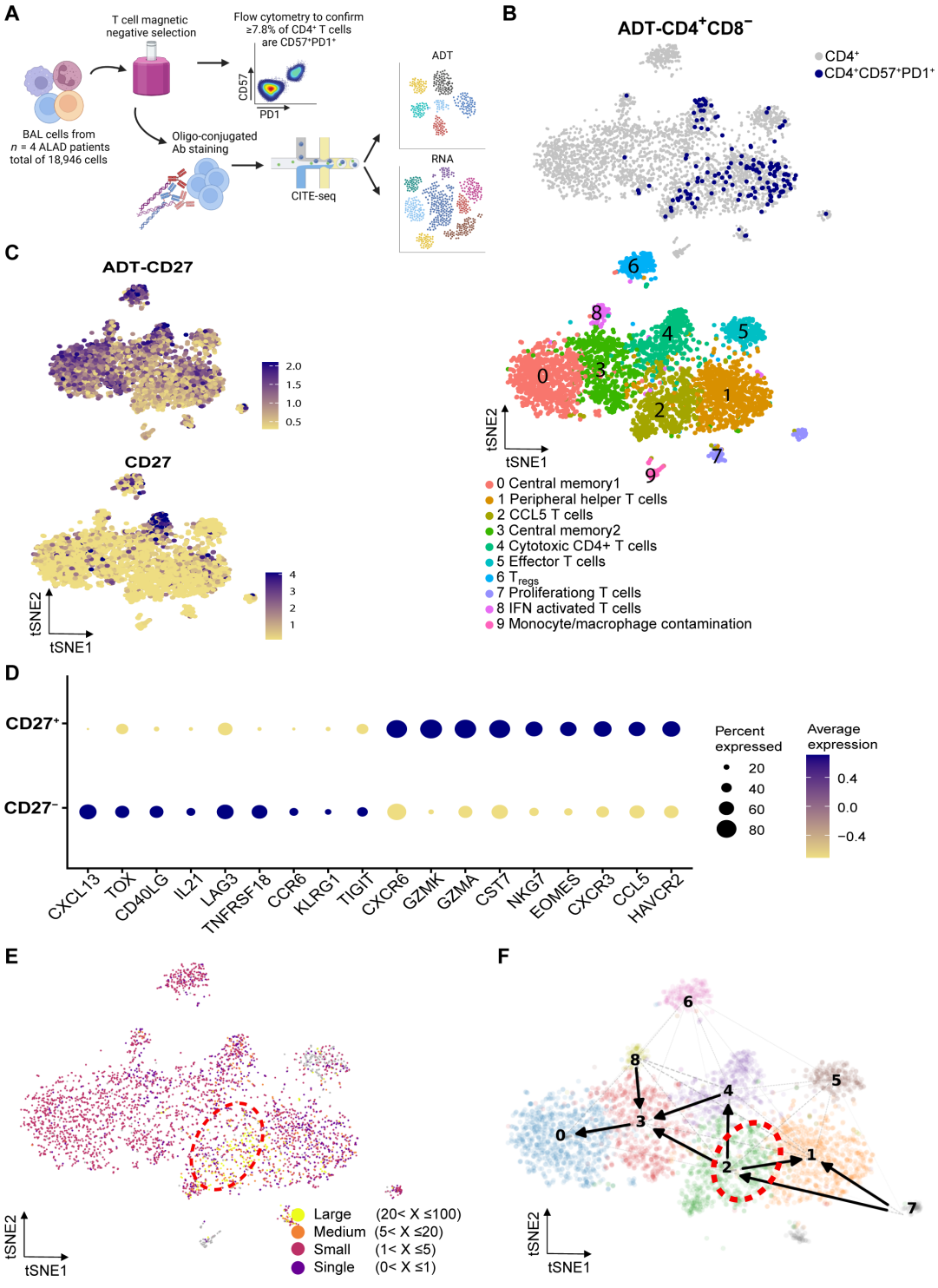

Fig. 5. Identification of distinct CD27$^+$ and CD27$^-$ subsets of CD4$^+$CD57$^+$PD1$^+$ T cells. (**A**) Four patients with ALAD were identified and T cells were enriched by magnetic negative selection. Flow cytometry was performed to confirm the presence of CD57$^+$PD1$^+$ T cells in the CD4$^+$ compartment. Cells underwent oligo-conjugated antibody (Ab) labeling (table S6) followed by CITE-seq. (**B**) After downsampling and integration, BAL CD4$^+$ T cells (CD3$^+$CD4$^+$CD8$^-$ identified by ADT) were displayed on tSNE plots. (Top) CD57 and PD1 expression (blue dots) on a feature plot showing all BAL CD4$^+$ cells. (Bottom) All 10 distinct cell clusters with corresponding annotations. (**C**) tSNE plots demonstrating CD27 protein [ADT-CD27 (top)] and RNA expression [*CD27* (bottom)]. (**D**) Dot plot of the selected top differentially expressed genes in BAL CD27$^+$ and CD27$^-$ CD4$^+$CD57$^+$PD1$^+$ T cells. Purple color indicates higher expression; dot size reflects the percentage of cells in each population expressing the gene. (**E**) tSNE plot overlaid with colors reflecting TCR clonal expansion. Red dotted circle indicates highly expanded clones within the CD27$^-$ population. (**F**) tSNE plot overlaid with RNA velocity trajectories (arrows). Red dotted circle shown in (D) is overlaid here, indicating the likely origin of CD4$^+$CD57$^+$PD1$^+$ T cells.

Functional analysis of CD4$^+$CD57$^+$PD1$^+$ T cells reveals features of inflammation and senescence

Considering the potential distinct functional properties—Tph, cytotoxic, and senescent—of CD4$^+$CD57$^+$PD1$^+$ T cells, we set out to characterize their functions in vitro. For this purpose, CD4$^+$ T cells from BAL samples of 15 LT recipients experiencing ALAD were sorted to obtain CD4$^+$CD57$^+$PD1$^+$ T cells and their CD4$^+$CD57$^-$PD1$^-$ counterparts (Fig. 6A). Fluorescence-activated cell sorting (FACS) data demonstrated that, in all cases, the CD57$^+$PD1$^+$ cell frequency was ≥7.8% of BAL CD4$^+$ T cells (Fig. 6B). On the basis of the hypothesis that CD4$^+$CD57$^+$PD1$^+$ T cells may be senescent, we predicted that sorted cells would exhibit decreased proliferation, enhanced cytokine secretion, and resistance to TCR restimulation-induced cell death (RICD) when compared to CD57$^-$PD1$^-$ cells.

Supernatants from cells stimulated overnight were collected and subjected to a multiplexed cytokine assay. This revealed that CD4$^+$CD57$^+$PD1$^+$ cells, compared to CD4$^+$CD57$^-$PD1$^-$ cells sorted from the same BAL samples, expressed more IL-21 and CXCL8; differences in IL-4 and granzyme A secretion were more variable (Fig. 6C). In conjunction with our CITE-seq data, these findings suggested that CD4$^+$CD57$^+$PD1$^+$ T cells may have Tph or cytotoxic properties, or both. Stimulated CD4$^+$CD57$^+$PD1$^+$ T cells and their CD57$^-$PD1$^-$ counterparts were then tested for proliferation, based on dilution of carboxyfluorescein diacetate succinimidyl ester (CFSE) (Fig. 6D). Proliferation data revealed that CD4$^+$CD57$^+$PD1$^+$ T cells exhibited significantly less proliferation compared to CD4$^+$CD57$^-$PD1$^-$ cells (Fig. 6E), in keeping with T cell senescence (*45*, *46*). Last, CD4$^+$CD57$^+$PD1$^+$ T cells were less susceptible to RICD compared to CD4$^+$CD57$^-$PD1$^-$ cells (Fig. 6, F and G). Together, these data imply that CD4$^+$CD57$^+$PD1$^+$ T cells are senescent but pro-inflammatory T cells that are resistant to antigen-induced death. These observations may help to explain the emergence of ALAD and CLAD in LT recipients despite potent triple-drug immunosuppression, which would be predicted to be less effective against these cells.

DISCUSSION

In this study, we used a high-dimensional mass cytometry discovery approach to identify a T cell population in LT recipient BAL that is associated with a heightened risk for future allograft dysfunction, failure, and death. The risk conferred by the appearance of CD4$^+$CD57$^+$PD1$^+$ T cells in the BAL remained elevated after bivariate adjustments for age, sex, and donor and recipient CMV serostatus mismatch.

In keeping with previous works examining LT recipient BAL, our samples contained a diversity of leukocyte populations. The prior studies demonstrated statistically significant relationships between BAL CD8$^+$ T cells, NK cells, eosinophils, T_{regs}, and outcomes in LT, but this has not led to meaningful improvements in clinical care because wide overlaps in the frequency distributions of these populations have meant that they lack discriminatory power in individual patients (*13*, *14*, *18*, *47*–*50*). In contrast, although CD4$^+$CD57$^+$PD1$^+$ T cells will require further validation in larger studies, their prevalence among CD4$^+$ T cells discriminated patients who remained stable from those about to undergo ALAD with high precision, in a discovery cohort, and confirmed in an independent validation cohort. Our observation therefore represents a promising biomarker that may, in the future, permit the selection of LT recipients for targeted preventative interventions.

A review of clinical and laboratory variables present at the time of each bronchoscopy did not reveal any clear association between the appearance of ≥7.8% of CD57$^+$PD1$^+$ T cells in the BAL CD4$^+$ T cell compartment and other indicators of lung allograft inflammation or dysfunction. This observation likely reflects the relatively poor performance of histopathologic and cytologic findings in the diagnosis of lung allograft rejection. Interpretation of transbronchial biopsy histology is fraught, with high rates of ungradable biopsies and substantial interobserver disagreement among pathologists (*7*, *8*). It is therefore perhaps not unexpected that bronchoscopies with high frequencies of CD4$^+$CD57$^+$PD1$^+$ T cells showed no particular association with histological rejection. Likewise, we found that this T cell population is not a marker of lung allograft infection because there were no differences in pathogen isolation from the same BAL samples. Our interpretation of these findings is that analysis of BAL CD4$^+$CD57$^+$PD1$^+$ T cells may markedly improve the utility of surveillance bronchoscopy after LT, which will require further evaluation in larger prospective studies.

Beyond their value as a biomarker of future allograft dysfunction, several lines of evidence suggest that CD4$^+$CD57$^+$PD1$^+$ T cells could be mechanistically relevant to the pathogenesis of chronic lung allograft rejection and fibrosis. First, our CITE-seq data indicate that most clonally expanded CD4$^+$ T cell populations in the BAL of patients with ALAD were CD57$^+$PD1$^+$, which indicates that these cells have undergone antigen-driven expansion in the lung. Furthermore, in addition to their appearance in BAL, we detected CD4$^+$CD57$^+$PD1$^+$ T cells in human explanted CLAD lung tissue obtained at the time of retransplantation. The cells were observed in proximity to B cells and small airways; coupled with the finding that the transcriptome and secretome of BAL CD4$^+$CD57$^+$PD1$^+$ T cells includes IL-21 and granzymes, this observation suggests that they may mediate allograft injury and/or subserve Tph functions. In support of this assertion, in our ischemia-reperfusion injury-augmented mouse model of human CLAD, we observed CD4$^+$CD57$^+$PD1$^+$ T cells in the lung allografts of mice with marked fibrotic pathology. In contrast, allografts with milder fibrosis did not contain many CD4$^+$CD57$^+$PD1$^+$ T cells. We have previously shown that fibrosis in this model is B cell dependent (*31*), and so in future work, it will be important to consider the possible existence of a CD4$^+$CD57$^+$PD1$^+$ T cell–B cell axis that drives chronic lung allograft rejection in mice and humans.

Accumulating evidence has revealed an association of CD4$^+$CD57$^+$ T cells, with or without associated PD1 expression, with autoimmune diseases, infectious diseases, and cancers (*51*). CD4$^+$CD57$^+$ T cells have been detected in the peripheral blood of kidney transplant recipients undergoing rejection (*52*), particularly in costimulation blockade resistant rejection (*53*, *54*). Of note, the CD4$^+$CD57$^+$ T cells associated with rejection in kidney transplantation were measured in the PBMC and exhibit low expression of PD1. In another study, Brugière and colleagues observed that the risk of CLAD was increased in patients with a high proportion of circulating CD4$^+$CD57$^+$ILT2$^+$ T cells, which could be inhibited by HLA-G (*55*). However, in that study, PD1 expression was not assessed, and the association with CLAD was not as strong as we report here. Therefore, it is unclear whether any of these peripheral CD4$^+$CD57$^+$ populations bear a functional resemblance or developmental relationship to those that we have described within lung allografts.

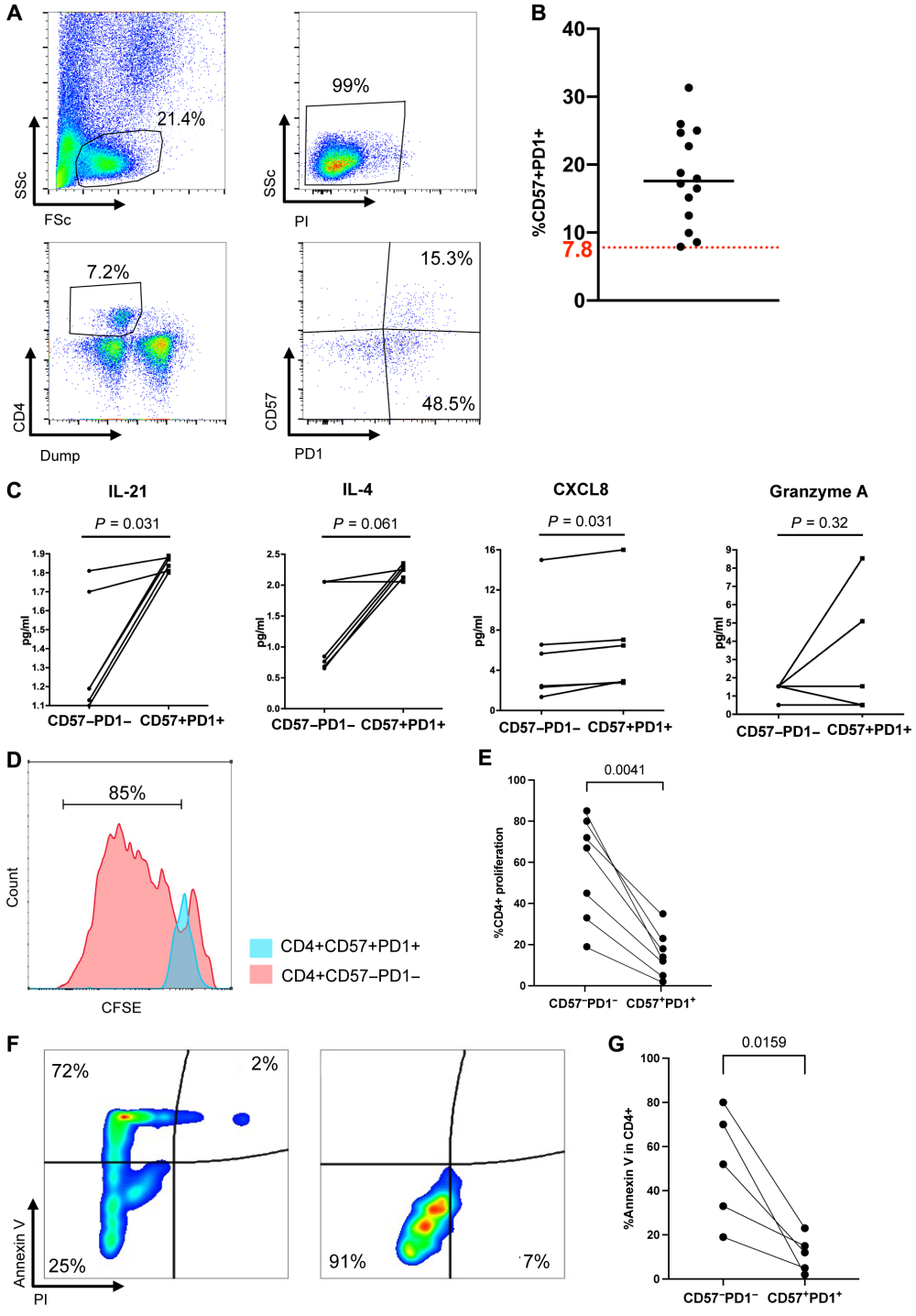

Fig. 6. Functional properties of CD4$^+$CD57$^+$PD1$^+$ T cells. (**A**) CD4$^+$CD57$^+$PD1$^+$ T cells can be identified by conventional flow cytometry. BAL cells were stained with CD4, CD57, and PD1 antibodies, and CD57$^+$PD1$^+$ cells were identified within the CD4$^+$ population, allowing quantification and cell sorting. (**B**) Percentage of CD57$^+$PD1$^+$ cells within the CD4$^+$ gate is shown for $n = 14$ patients with ALAD. (**C**) Sorted CD57$^+$PD1$^+$ and CD57$^-$PD1$^-$ CD4$^+$ T cells from ALAD BAL samples were stimulated in vitro with anti-CD3/anti-CD28 antibodies overnight. Culture supernatants were subjected to multiplexed cytokine quantification. IL-21 ($P = 0.031$), IL-4 ($P = 0.062$), CXCL8 (IL-8, $P = 0.031$), and GZMA ($P = 0.062$) were generally secreted in greater concentrations by CD57$^+$PD1$^+$ T cells than their CD57$^-$PD1$^-$ counterparts, Wilcoxon matched-pairs signed-rank tests. (**D**) Sorted CD57$^+$PD1$^+$ (blue) and CD57$^-$PD1$^-$ CD4$^+$ (pink) T cells from ALAD BAL were examined for proliferation in response to CD3/CD28 stimulation by dilution of CFSE. (**E**) The percentage of CD57$^+$PD1$^+$ T cells undergoing proliferation was lower compared to that of their CD57$^-$PD1$^-$ counterparts. Linked CD57$^+$PD1$^+$ and CD57$^-$PD1$^-$ cells are sorted from the same LT recipient. Wilcoxon matched-pairs signed-rank test, $P = 0.0041$. (**F**) Sorted CD57$^+$PD1$^+$ T cells (right) and their CD57$^-$PD1$^-$ counterparts (left) were subjected to RICD. Annexin V and PI staining is shown. (**G**) Annexin V staining was lower in CD57$^+$PD1$^+$ T cells compared to their CD57$^-$PD1$^-$ counterparts. Linked CD57$^+$PD1$^+$ and CD57$^-$PD1$^-$ T cells are sorted from the same LT recipient. Wilcoxon matched-pairs signed-rank test, $P = 0.0159$.

Moreover, although peripheral blood $CD57^+$ T cells are also reported to reflect CMV infection and/or age (*56*), our patients' characteristics did not suggest any association between age and/or CMV seropositivity with $CD4^+CD57^+PD1^+$ T cells.

PD1 expression by $CD8^+$ T cells in tumor microenvironments is associated with cancer progression and generally reflects a state of exhaustion in which effector functions are deactivated. BAL $CD4^+CD57^+PD1^+$ T cells also expressed several additional molecules that have been associated with exhaustion, including *HAVCR2*, *LAG3*, and *CTLA4*. Although analysis of the cells ex vivo revealed that they were both hypoproliferative and resistant to T cell RICD, their production of inflammatory cytokines, which is not a feature of exhaustion, suggests that they are senescent rather than exhausted. Of note, senescent $CD4^+$ and $CD8^+$ T cells in humans were described as having the phenotype $CD45RA^+KLRG1^+CD57^+CD28^-CD27^-$ (*57*, *58*). Animal and human data indicate that senescent T cells participate in other chronic inflammatory, degenerative, and metabolic disorders (*46*). Last, our data suggest that $CD4^+CD57^+PD1^+$ also have some features in common with Trm cells, which have previously been identified in transplanted lungs (*41*). Additional work to confirm these observations will be required.

LT recipients typically receive immunosuppressive drugs—calcineurin inhibitors, corticosteroids, and antimetabolites—in much higher doses than other solid organ transplant recipients and yet also have the highest rates of acute and chronic allograft rejection. With respect to T cells, these drugs act by inhibiting cell proliferation. In this context, we speculate that $CD4^+CD57^+PD1^+$ T cells, which exhibit reduced proliferation, escape this inhibition and can continue to produce cytokines. Further work will be required to understand how these cells arise within the lung allograft, whether they mediate graft injury, and whether specific targeting of these cells may have a therapeutic benefit.

METHODS

Study design and BAL collection

The samples analyzed in this study were collected with informed consent for research use and were approved by the University Health Network Research Ethics Board (15-9531). BAL cells from 50 TLTP LT recipients presenting for surveillance bronchoscopy at 3 months posttransplant were obtained according to a standard protocol (*59*). In addition, for each LT recipient, two further samples were obtained from each recipient to form a longitudinal cohort (fig. S1). Cells were centrifuged at 400*g* for 5 min and resuspended in 1 ml of 10% dimethyl sulfoxide/90% fetal bovine serum (FBS) for viable cryopreservation. Cryovials were placed in Mr. Frosty containers at −80°C for 24 hours and then stored in liquid nitrogen until thawing for processing and CyTOF. BAL cells from a further 14 LT recipients with ALAD (defined as a decrease in the FEV1 by 10% or more from the baseline FEV1 measurements) were used for sorting fresh $CD4^+CD57^+PD1^+$ T cells and their $CD57^-PD1^-$ counterparts for functional analyses.

Time-of-flight mass cytometry

Metal-conjugated antibodies were purchased either preconjugated from Fluidigm or purified from BioLegend, Thermo Fisher Scientific, or BD Biosciences and subsequently conjugated to metals using Maxpar Antibody Labeling Kits (Fluidigm) according to the manufacturer's instructions (table S1). Cryopreserved BAL cells were recovered and divided into stimulated [with phorbol 12-myristate 13-acetate (50 ng/ml) and ionomycin (500 ng/ml)] and unstimulated conditions to allow analysis of cytokine secretion expression and surface markers. Cells were incubated with a cocktail of antibodies against cell surface molecules for 30 min at room temperature. After treatment with intracellular fixation and permeabilization buffers (BD Biosciences), cells were incubated with metal-conjugated antibodies against intracellular proteins. Cells were then washed and stained with Intercalator-Ir (Fluidigm) diluted in phosphate-buffered saline (PBS) containing 1.6% paraformaldehyde and stored at 4°C until next-day acquisition. To assess variation between mass cytometry runs, a control healthy volunteer PBMC sample was aliquoted, recovered, and stained and analyzed alongside the BAL samples.

CyTOF data analysis

CyTOF data were initially analyzed with manual gating to exclude debris, dead cells, and doublets and to select $CD45^+$ cells using Cytobank software (Beckman Coulter). We then used the FlowSOM and viSNE algorithms (5000 iterations, perplexity = 100) for visualization of high-dimensional data (*20*, *60*). Subsequently, we applied CITRUS (*21*) on the $CD3^+$ population from the discovery cohort (n = 25; table S2) to identify cell subsets associated with ALAD within 90 days of the sample. CITRUS was run 10 times with an "equal number" of cells per sample, looking for cluster "abundance" (normalized to the number of $CD45^+$ cells in each sample), with a 1% false discovery rate (*21*) according to the Benjamini-Hochberg method (*61*). To incorporate the time-course design of our study, we implemented a GLMM analysis–adapted R pipeline as described by Nowicka and colleagues (*22*). In this approach, different time points for each LT recipient were defined as a variable to allow intrasubject pairing. Last, we used manual gating to confirm the results of CITRUS and GLMM analysis.

Imaging mass cytometry

Lung tissue samples were obtained during retransplantation procedures from eight patients who underwent retransplantation due to end-stage CLAD between 2015 and 2018 (*29*). A single biopsy was obtained from the upper lobe of each explanted sample. The harvested lung tissue was inflated and immersed in a 10% formalin solution for 24 hours prior to immersion in a 70% ethanol solution for an additional 24-hour period. Samples were then embedded in paraffin. Four-micrometer-thick sections of paraffin-embedded lung tissue were prepared and affixed to slides for further analysis. In addition to the CLAD patient samples, we included control samples in our study. Controls included lung tissue samples from two lobectomy procedures for suspected cancer and excess tissue from two donor lungs collected at the end of the cold ischemic phase of preservation. Sections of CLAD and control lung tissue were stained with a panel of 35 heavy metal–tagged antibodies (table S6). Three 1 mm–by–1 mm regions of interest (ROIs) were selected on adjacent hematoxylin and eosin–stained sections of each sample by centering the field of view on an airway, with the goal of having three different airway sizes represented in each sample (>600, 300 to 600, and <300 μm in diameter). ROIs were subjected to ablation using the Hyperion Imaging System (Fluidigm) using a laser frequency of 200 Hz, with laser power ranging from 3.5 to 4.5. The median number of cells per ROI was 5540 (interquartile range, 3845 to 7577) in the

CLAD lusngs and 4961 (interquartile range, 4138 to 5397) in control lungs. The ablation procedure generated files in both .txt and .mcd formats, which were subsequently subjected to thorough analysis using the Histocat software platform (*30*). Other data from these analyses are reported elsewhere (*29*).

Animal model

Orthotopic LT was performed using C57BL/10 donors and C57BL/6 recipients under different graft preservation conditions as described previously (*31*). Briefly, harvested lungs were stored either under minimal (60 min at 4°C followed by 15 min of warm anastomotic time) or prolonged (6 hours at 4°C, 45 min at 37°C, followed by 15 min of warm anastomotic time) storage prior to reperfusion. The animal protocol (4378) was approved by the University Health Network Animal Care Committee, and all experiments were conducted in accordance with the regulations of the Canadian Council on Animal Care.

Orthotopic LT recipients were euthanized 28 days after LT for histological analysis and cellular phenotyping. Grafts were flushed with saline and digested with collagenase A and DNase I in a gentleMACS tissue dissociator (Miltenyi Biotec). Cells were stained with cocktails of fluorochrome-conjugated monoclonal antibodies including AF647-conjugated anti-mouse CD57 (polyclonal; Bioss) and AF488-conjugated anti-mouse PD1 (polyclonal; Bioss). Flow cytometry data were analyzed using FlowJo (v10, FlowJo LLC) and correlated with histological grading. We graded peribronchial fibrosis and parenchymal fibrosis in a blinded manner according to a published scoring system (*32*). Immunofluorescence staining of sections of formalin-fixed and paraffin-embedded lung tissue was conducted by antigen retrieval using 1x pH 9 Tris/EDTA buffer before staining with unconjugated anti-mouse CD4. This was followed by a secondary antibody cocktail including Alexa Fluor 555 anti-rabbit IgG (A-31572, Invitrogen) as well as AF647-conjugated anti-mouse CD57 (polyclonal; Bioss) and AF488-conjugated anti-mouse PD1 (polyclonal; Bioss). Nuclei were stained with 4′,6-diamidino-2-phenylindole (DAPI), and immunofluorescence images were acquired using a Zeiss AxioObserver.

CITE-seq sample processing and acquisition

We identified four LT recipients scheduled for bronchoscopy with ALAD (FEV1 decrease by ≥10% from the prior value). Fresh BAL cells were collected by centrifugation at 400*g* for 5 min. T cells were obtained using a $CD3^+$ T cell enrichment kit (EasySep Human T Cell enrichment, STEMCELL Technologies) according to the manufacturer's instructions. Enriched T cells were resuspended at 1×10^6 cells/ml in PBS + 0.05% bovine serum albumin (BSA). Fifty microliters of the cell suspension was stained with BV711 conjugated anti-human CD4, allophycocyanin (APC)-conjugated anti-human PD1, and phycoerythrin-cyanine 7 (PE-Cy7) anti-human CD57 and analyzed by flow cytometry to confirm ≥7.8% of $CD57^+PD1^+$ cells in the BAL $CD4^+$ T cell compartment. If confirmed, the remaining cells were used for CITE-seq. Briefly, 1×10^6 cells were resuspended in 45 μl of PBS + 0.05% BSA before adding 5 μl of Fc blocking reagent and incubated for 10 min at 4°C. TotalSeq-C antibody cocktails were prepared during the incubation by adding predetermined concentrations of each antibody (table S6). The resulting cocktail was then added to cells and incubated for 30 min at 4°C. After incubation, the cell pellets were resuspended in 1 ml of PBS + 0.05% BSA and centrifuged for 5 min at 400*g*. After a total of three washes, the final cell density was adjusted to 1000 to 1200 cells/μl and subjected to the 10X Genomics Chromium 5′ Immune Profiling v2.0 protocol for library preparation. A total of 2×10^4 cells from each sample were loaded onto a 10X single cell G chip. After droplet generation, samples were transferred to a prechilled 96-well plate (Eppendorf), heat sealed, and incubated overnight in a Veriti 96-well thermocycler (Thermo Fisher Scientific). The next day, sample cDNA was recovered using Recovery Agent (10X Genomics) and subsequently cleaned up using Silane DynaBeads (Thermo Fisher Scientific) mix as outlined by the user guide 5′ Immune Profiling v2.0. Purified cDNA was amplified for 11 cycles before being cleaned up using SPRIselect beads (Beckman Coulter). Samples were diluted 9:1 [elution buffer (Qiagen):cDNA] and run on a Bioanalyzer (Agilent Technologies) to determine the cDNA concentration. The library was then sequenced using an Illumina Novaseq 6000 sequencer using the following parameters: Read 1: 28 base pairs (bp), Index 1: 10 bp, Index 2: 10 bp, and Read 2: 90 bp.

CITE-seq analysis

The sequencing output was first demultiplexed and converted into FASTQ files using Cell Ranger (*62*). Reads were aligned to the human reference genome (grch38), and count unique molecular identifiers (UMIs) in the mRNA libraries, and CITE-seq-Count to count UMIs in the ADT libraries. The matrix, barcodes, and gene information from Cell Ranger were then used to create gene-cell matrices and a Seurat object (*63*). For each Seurat object, cells with poor quality were excluded based on the following quality control metrics: unique gene counts over 5000 or below 200, UMI counts over 30,000, and mitochondrial gene expression higher than 10%. Each sample was scaled and normalized using Seurat's "SCTransform" function followed by adding the protein expression levels to the Seurat object and normalization and scaling for ADT assay. Next, $CD4^+$ T cells were subset based on high CD4 and low CD8 protein expression (ADT-CD8 < 12 and ADT-CD4 > 12). Seurat objects of $CD4^+$ cells from all four BAL samples were merged into a single Seurat object. The SCTransform method was used for normalization, scaling, and integration, which corrects for unwanted sources of variation and enhances the signal of genuine biological differences between cells (*64*). Then, dimensionality reduction was applied to the integrated Seurat object, allowing visualization and interpretation of the high-dimensional scRNA-seq data. This was followed by unsupervised clustering (resolution = 0.5), which led to the identification of 10 clusters. Then, cells with higher expression of protein level of CD57 and PD1 were highlighted on a t-distributed stochastic neighbor embedding (tSNE) plot.

The donor or recipient origin of individual cells was inferred from SNVs in the expressed transcriptome using scTx (*34*). A second genotype in a cell sample is identified by clustering cells based on allele fraction distances in multidimensional space; if a second genotype is not found, the algorithm searches for very low frequency cells of a second genotype using a genotype score metric. If neither method identifies a second genotype, the algorithm concludes that a second genotype is not present. Ascertainment of cell origin is inferred by the assumption that most epithelial cells [~90% in lung allografts (*65*)] are likely to be donor derived.

RNA velocity estimates the future state of individual cells by calculating the ratio of unspliced to spliced mRNA for each gene. The spliced and unspliced counts from the scRNA-seq data were used to

calculate RNA velocity using the velocyto package in Python (*66*). Splicing information extracted from velocyto was then added to all the selected cells in the $CD4^+$ Seurat object. Subsequently, $CD4^+$ T cells underwent pseudotime trajectory analysis using the scVelo pipeline (*67*). This analysis inferred the trajectory and the chronological sequence of cell states, highlighting the differentiation paths taken by cells. The pseudotime values were visualized on the tSNE plots, providing insights into the dynamic processes and cellular transitions at play.

Fluorescence-activated cell sorting

BAL cells were collected from 15 ALAD samples and stained with fluorophore-tagged surface antibodies for 30 min at room temperature. The following antibodies were used to stain the cells: BV711-conjugated anti-human CD4 (BioLegend); APC-conjugated anti-human PD1 (BioLegend); and PE/Cy7-conjugated anti-human CD57, in addition to biotinylated CD163, CD14, CD8, and CD56 (all from BioLegend). Cells washed with 500 µl of 1% FBS in PBS and incubated with streptavidin-AF488 (1:200, BioLegend) for 20 min, before washing and staining with propidium iodide (PI) to identify dead cells. Stained cells were subjected to FACS using a Sony SH800 instrument. After exclusion of PI-positive cells and putative doublets based on forward and side scatter analysis, cells in the dump channel (AF488) were eliminated. The remaining cells were gated to select $CD4^+$ T cells and sorted for $CD57^+PD1^+$ and $CD57^-PD1^-$ cells.

Cell culture, multiplex protein analysis, and in vitro assays

Sorted cells were labeled with 1 µM CFSE in serum-free PBS prior to wash and culture with plate-bound anti-CD3 (5 µM) and soluble anti-CD28 (1 µM) antibodies in Dulbecco's modified Eagle's medium containing 5.55 mM D-glucose, 4 mM L-glutamine, and 1 mM sodium pyruvate, supplemented with 10% FBS, penicillin (50 U/ml), and streptomycin (50 mg/ml) and human recombinant IL-2 (500 U/ml; Proleukin, Chiron). After 18 hours, 100 µl of supernatant was replaced with fresh media. The collected supernatant was stored at −80°C for later multiplex analysis. Supernatants were thawed and subjected to a custom multiplex bead kit (R&D Systems) to assess the levels of released analytes including IL-21, IL-4, CXCL8, and granzyme A. Samples were prepared in a 1:1 dilution with assay buffer, as suggested by the manufacturer. Diluted samples and standards were run in duplicate. Biomarker concentrations were obtained using a Bio-Plex MAGPIX Multiplex Reader (Bio-Rad). All samples and standards were run in duplicate according to the manufacturer's protocols.

After 5 days, CFSE dilution in the sorted cells, a measure of T cell proliferation, was determined by flow cytometry. Last, an RICD assay (*68*) was used to assess whether $CD57^+PD1^+$ cells are less susceptible to this mode of cell death than their $CD57^-PD1^-$ counterparts. $CD57^+PD1^+$ and $CD57^-PD1^-$ cells were stimulated in culture for 7 days before washing and were then restimulated with anti-CD3 mAb (OKT3, 100 ng/ml final) for 24 hours. Cells were then harvested and stained with annexin V and PI for evaluation of apoptotic cell death.

Statistics

All statistical tests were two-sided unless stated otherwise. The Wilcoxon rank sum test was used to assess statistical differences between two groups. When assessing >2 groups simultaneously, the nonparametric Kruskal-Wallis test was used. A Fisher's exact test was applied to assess statistical differences between two categorical variables. ROC curves were used to assess classification accuracy, which was quantified by the area under the curve (AUC). Kaplan-Meier plots and two-sided log-rank tests were used to compare survival probabilities between groups. Cox proportional hazards regression models were used to adjust for potential confounders for time-to-CLAD or time-to-death/retransplantation analysis, and Cox regression analyses were used to assess covariates with respect to time-to-allograft dysfunction. All statistical analyses were performed using R v.3.5.1+ or Prism 8+ (GraphPad Software).

Supplementary Materials

This PDF file includes:

Figs. S1 to S11
Tables S1 to S6

REFERENCES AND NOTES

1. J. M. Ali, E. M. Bolton, J. A. Bradley, G. J. Pettigrew, Allorecognition pathways in transplant rejection and tolerance. *Transplantation* **96**, 681–688 (2013).
2. D. C. Chambers, M. Perch, A. Zuckermann, W. S. Cherikh, M. O. Harhay, D. Hayes Jr., E. Hsich, K. K. Khush, L. Potena, A. Sadavarte, K. Lindblad, T. P. Singh, J. Stehlik, International Society for Heart and Lung Transplantation, The International Thoracic Organ Transplant Registry of the International Society for Heart and Lung Transplantation: Thirty-eighth adult lung transplantation report—2021; Focus on recipient characteristics. *J. Heart Lung Transplant.* **40**, 1060–1072 (2021).
3. M. Kawashima, S. C. Juvet, The role of innate immunity in the long-term outcome of lung transplantation. *Ann. Transl. Med.* **8**, 412 (2020).
4. K. Bando, I. L. Paradis, S. Similo, H. Konishi, K. Komatsu, T. G. Zullo, S. A. Yousem, J. M. Close, A. Zeevi, R. J. Duquesnoy, J. Manzetti, R. J. Keenan, J. M. Armitage, R. L. Hardesty, B. P. Griffith, Obliterative bronchiolitis after lung and heart-lung transplantation: An analysis of risk factors and management. *J. Thorac. Cardiovasc. Surg.* **110**, 4–14 (1995).
5. D. Heng, L. D. Sharples, K. McNeil, S. Stewart, T. Wreghitt, J. Wallwork, Bronchiolitis obliterans syndrome: Incidence, natural history, prognosis, and risk factors. *J. Heart Lung Transplant.* **17**, 1255–1263 (1998).
6. S. Moshkelgosha, A. Duong, G. Wilson, T. Andrews, G. Berra, B. Renaud-Picard, M. Liu, S. Keshavjee, S. MacParland, J. Yeung, T. Martinu, S. Juvet, Interferon-stimulated and metallothionein-expressing macrophages are associated with acute and chronic allograft dysfunction after lung transplantation. *J. Heart Lung Transplant.* **41**, 1556–1569 (2022).
7. S. M. Bhorade, A. N. Husain, C. Liao, L. C. Li, V. N. Ahya, M. A. Baz, V. G. Valentine, R. B. Love, H. Seethamraju, C. G. Alex, R. Bag, N. C. DeOliveira, W. T. Vigneswaran, E. R. Garrity, S. M. Arcasoy, Interobserver variability in grading transbronchial lung biopsy specimens after lung transplantation. *Chest* **143**, 1717–1724 (2013).
8. A. Stephenson, J. Flint, J. English, S. Vedal, G. Fradet, D. Chittock, R. D. Levy, Interpretation of transbronchial lung biopsies from lung transplant recipients: Inter- and intraobserver agreement. *Can. Respir. J.* **12**, 75–77 (2005).
9. L. Levy, A. Tigert, E. Huszti, T. Saito, N. Mitsakakis, S. Moshkelgosha, B. Joe, K. M. Boonstra, J. M. Tikkanen, S. Keshavjee, S. C. Juvet, T. Martinu, Epithelial cell death markers in bronchoalveolar lavage correlate with chronic lung allograft dysfunction subtypes and survival in lung transplant recipients-a single-center retrospective cohort study. *Transpl. Int.* **32**, 965–973 (2019).
10. S. Moshkelgosha, L. Levy, T. Martinu, B. Joe, C. Guidos, S. Keshavjee, S. C. Juvet, Paper presented at the International Society of Heart and Lung Transplantation 38th Annual Meeting, Nice, France, 11 to 14 April 2018.
11. S. Moshkelgosha, L. Levy, T. Martinu, R. Zamel, C. Guidos, S. Keshavjee, J. Yeung, S. C. Juvet, Paper presented at the International Society for Heart and Lung Transplantation 39th Annual Meeting, Orlando, FL, 3 to 6 April 2019.
12. S. Moshkelgosha, L. Levy, G. W. Wilson, T. Martinu, S. Keshavjee, J. Yeung, S. C. Juvet, Paper presented at the International Society of Heart and Lung Transplantation 40th Annual Meeting, Montreal, Canada, 22 to 25 April 2020.
13. B. F. Whitehead, C. Stoehr, C. Finkle, G. Patterson, J. Theodore, C. Clayberger, V. A. Starnes, Analysis of bronchoalveolar lavage from human lung transplant recipients by flow cytometry. *Respir. Med.* **89**, 27–34 (1995).
14. M. Reynaud-Gaubert, P. Thomas, R. Gregoire, M. Badier, P. Cau, J. Sampol, R. Giudicelli, P. Fuentes, Clinical utility of bronchoalveolar lavage cell phenotype analyses in the

postoperative monitoring of lung transplant recipients. *Eur. J. Cardiothorac. Surg.* **21**, 60–66 (2002).
15. S. Hodge, G. Hodge, J. Ahern, C. L. Liew, P. Hopkins, D. C. Chambers, P. N. Reynolds, M. Holmes, Increased levels of T cell granzyme b in bronchiolitis obliterans syndrome are not suppressed adequately by current immunosuppressive regimens. *Clin. Exp. Immunol.* **158**, 230–236 (2009).
16. D. C. Neujahr, A. C. Cardona, O. Ulukpo, M. Rigby, A. Pelaez, A. Ramirez, A. A. Gal, S. D. Force, E. C. Lawrence, A. D. Kirk, C. P. Larsen, Dynamics of human regulatory T cells in lung lavages of lung transplant recipients. *Transplantation* **88**, 521–527 (2009).
17. S. J. Hodge, G. L. Hodge, P. N. Reynolds, M. D. Holmes, Differential rates of apoptosis in bronchoalveolar lavage and blood of lung transplant patients. *J. Heart Lung Transpl.* **24**, 1305–1314 (2005).
18. J. R. Greenland, N. P. Jewell, M. Gottschall, N. N. Trivedi, J. Kukreja, S. R. Hays, J. P. Singer, J. A. Golden, G. H. Caughey, Bronchoalveolar lavage cell immunophenotyping facilitates diagnosis of lung allograft rejection. *Am. J. Transpl.* **14**, 831–840 (2014).
19. D. R. Bandura, V. I. Baranov, O. I. Ornatsky, A. Antonov, R. Kinach, X. Lou, S. Pavlov, S. Vorobiev, J. E. Dick, S. D. Tanner, Mass cytometry: Technique for real time single cell multitarget immunoassay based on inductively coupled plasma time-of-flight mass spectrometry. *Anal. Chem.* **81**, 6813–6822 (2009).
20. S. Van Gassen, B. Callebaut, M. J. Van Helden, B. N. Lambrecht, P. Demeester, T. Dhaene, Y. Saeys, FlowSOM: Using self-organizing maps for visualization and interpretation of cytometry data. *Cytometry A* **87**, 636–645 (2015).
21. R. V. Bruggner, B. Bodenmiller, D. L. Dill, R. J. Tibshirani, G. P. Nolan, Automated identification of stratifying signatures in cellular subpopulations. *Proc. Natl. Acad. Sci. U.S.A.* **111**, E2770–E2777 (2014).
22. M. Nowicka, C. Krieg, L. M. Weber, F. J. Hartmann, S. Guglietta, B. Becher, M. P. Levesque, M. D. Robinson, CyTOF workflow: Differential discovery in high-throughput high-dimensional cytometry datasets. *F1000Res.* **6**, 748 (2017).
23. M. Cypel, J. C. Yeung, M. Liu, M. Anraku, F. Chen, W. Karolak, M. Sato, J. Laratta, S. Azad, M. Madonik, C. W. Chow, C. Chaparro, M. Hutcheon, L. G. Singer, A. S. Slutsky, K. Yasufuku, M. de Perrot, A. F. Pierre, T. K. Waddell, S. Keshavjee, Normothermic ex vivo lung perfusion in clinical lung transplantation. *N. Engl. J. Med.* **364**, 1431–1440 (2011).
24. J. P. Stone, H. Sevenoaks, T. Sjoberg, S. Steen, N. Yonan, J. E. Fildes, Mechanical removal of dendritic cell-generating non-classical monocytes via ex vivo lung perfusion. *J. Heart Lung Transpl.* **33**, 864–869 (2014).
25. C. Divithotawela, M. Cypel, T. Martinu, L. G. Singer, M. Binnie, C. W. Chow, C. Chaparro, T. K. Waddell, M. de Perrot, A. Pierre, K. Yasufuku, J. C. Yeung, L. Donahoe, S. Keshavjee, J. M. Tikkanen, Long-term outcomes of lung transplant with ex vivo lung perfusion. *JAMA Surg.* **154**, 1143–1150 (2019).
26. J. M. Tikkanen, L. G. Singer, S. J. Kim, Y. Li, M. Binnie, C. Chaparro, C. W. Chow, T. Martinu, S. Azad, S. Keshavjee, K. Tinckam, De novo DQ donor-specific antibodies are associated with chronic lung allograft dysfunction after lung transplantation. *Am. J. Respir. Crit. Care Med.* **194**, 596–606 (2016).
27. B. Renaud-Picard, M. Cheung, S. Moshkelgosha, G. Berra, D. Hwang, D. Hedley, S. Juvet, T. Martinu, Imaging mass cytometry for detailed cellular and spatial characterization of chronic lung allograft dysfunction (CLAD). *J. Heart Lung Transpl.* **41**, S106 (2022).
28. C. Giesen, H. A. Wang, D. Schapiro, N. Zivanovic, A. Jacobs, B. Hattendorf, P. J. Schuffler, D. Grolimund, J. M. Buhmann, S. Brandt, Z. Varga, P. J. Wild, D. Gunther, B. Bodenmiller, Highly multiplexed imaging of tumor tissues with subcellular resolution by mass cytometry. *Nat. Methods* **11**, 417–422 (2014).
29. B. Renaud-Picard, S. Moshkelgosha, G. Berra, M. Cheung, D. Hwang, D. Hedley, S. Juvet, T. Martinu, Detailed cellular and spatial characterization of chronic lung allograft dysfunction using imaging mass cytometry. *J. Heart Lung Transpl.* **44**, 118–124 (2024).
30. D. Schapiro, H. W. Jackson, S. Raghuraman, J. R. Fischer, V. R. T. Zanotelli, D. Schulz, C. Giesen, R. Catena, Z. Varga, B. Bodenmiller, histoCAT: Analysis of cell phenotypes and interactions in multiplex image cytometry data. *Nat. Methods* **14**, 873–876 (2017).
31. T. Watanabe, T. Martinu, A. Chruscinski, K. Boonstra, B. Joe, M. Horie, Z. Guan, K. F. Bei, D. M. Hwang, M. Liu, S. Keshavjee, S. C. Juvet, A B cell-dependent pathway drives chronic lung allograft rejection after ischemia-reperfusion injury in mice. *Am. J. Transplant* **19**, 3377–3389 (2019).
32. T. Martinu, H. Oishi, S. C. Juvet, M. Cypel, M. Liu, G. J. Berry, D. M. Hwang, S. Keshavjee, Spectrum of chronic lung allograft pathology in a mouse minor-mismatched orthotopic lung transplant model. *Am. J. Transplant* **19**, 247–258 (2019).
33. M. Stoeckius, C. Hafemeister, W. Stephenson, B. Houck-Loomis, P. K. Chattopadhyay, H. Swerdlow, R. Satija, P. Smibert, Simultaneous epitope and transcriptome measurement in single cells. *Nat. Methods* **14**, 865–868 (2017).
34. G. W. Wilson, A. Duong, S. Moshkelgosha, G. Bader, S. Keshavjee, T. Martinu, S. C. Juvet, J. C. Yeung, Robust segregation of donor and recipient cells from single-cell RNA-sequencing of transplant samples. *Front. Transplant* **2**, 1161146 (2023).
35. D. A. Rao, M. F. Gurish, J. L. Marshall, K. Slowikowski, C. Y. Fonseka, Y. Liu, L. T. Donlin, L. A. Henderson, K. Wei, F. Mizoguchi, N. C. Teslovich, M. E. Weinblatt, E. M. Massarotti, J. S. Coblyn, S. M. Helfgott, Y. C. Lee, D. J. Todd, V. P. Bykerk, S. M. Goodman, A. B. Pernis, L. B. Ivashkiv, E. W. Karlson, P. A. Nigrovic, A. Filer, C. D. Buckley, J. A. Lederer, S. Raychaudhuri, M. B. Brenner, Pathologically expanded peripheral T helper cell subset drives B cells in rheumatoid arthritis. *Nature* **542**, 110–114 (2017).
36. A. Manzo, B. Vitolo, F. Humby, R. Caporali, D. Jarrossay, F. Dell'accio, L. Ciardelli, M. Uguccioni, C. Montecucco, C. Pitzalis, Mature antigen-experienced T helper cells synthesize and secrete the B cell chemoattractant CXCL13 in the inflammatory environment of the rheumatoid joint. *Arthritis Rheum.* **58**, 3377–3387 (2008).
37. Y. Huang, X. Ba, L. Han, H. Wang, W. Lin, Z. Chen, S. Tu, T peripheral helper cells in autoimmune diseases: What do we know? *Front. Immunol.* **14**, 1145573 (2023).
38. S. S. Ng, F. De Labastida Rivera, J. Yan, D. Corvino, I. Das, P. Zhang, R. Kuns, S. B. Chauhan, J. Hou, X. Y. Li, T. C. M. Frame, B. A. McEnroe, E. Moore, J. Na, J. A. Engel, M. S. F. Soon, B. Singh, A. J. Kueh, M. J. Herold, M. Montes de Oca, S. S. Singh, P. T. Bunn, A. R. Aguilera, M. Casey, M. Braun, N. Ghazanfari, S. Wani, Y. Wang, F. H. Amante, C. L. Edwards, A. Haque, W. C. Dougall, O. P. Singh, A. G. Baxter, M. W. L. Teng, A. Loukas, N. L. Daly, N. Cloonan, M. A. Degli-Esposti, J. Uzonna, W. R. Heath, T. Bald, S.-K. Tey, K. Nakamura, G. R. Hill, R. Kumar, S. Sundar, M. J. Smyth, C. R. Engwerda, The NK cell granule protein NKG7 regulates cytotoxic granule exocytosis and inflammation. *Nat. Immunol.* **21**, 1205–1218 (2020).
39. A. N. Wein, S. R. McMaster, S. Takamura, P. R. Dunbar, E. K. Cartwright, S. L. Hayward, D. T. McManus, T. Shimaoka, S. Ueha, T. Tsukui, T. Masumoto, M. Kurachi, K. Matsushima, J. E. Kohlmeier, CXCR6 regulates localization of tissue-resident memory CD8 T cells to the airways. *J. Exp. Med.* **216**, 2748–2762 (2019).
40. B. V. Kumar, W. Ma, M. Miron, T. Granot, R. S. Guyer, D. J. Carpenter, T. Senda, X. Sun, S.-H. Ho, H. Lerner, A. L. Friedman, Y. Shen, D. L. Farber, Human tissue-resident memory T cells are defined by core transcriptional and functional signatures in lymphoid and mucosal sites. *Cell Rep.* **20**, 2921–2934 (2017).
41. M. E. Snyder, M. O. Finlayson, T. J. Connors, P. Dogra, T. Senda, E. Bush, D. Carpenter, C. Marboe, L. Benvenuto, L. Shah, H. Robbins, J. L. Hook, M. Sykes, F. D'Ovidio, M. Bacchetta, J. R. Sonett, D. J. Lederer, S. Arcasoy, P. A. Sims, D. L. Farber, Generation and persistence of human tissue-resident memory T cells in lung transplantation. *Sci. Immunol.* **4**, eaav5581 (2019).
42. G. Milardi, B. Di Lorenzo, J. Gerosa, F. Barzaghi, G. Di Matteo, M. Omrani, T. Jofra, I. Merelli, M. Barcella, M. Filippini, A. Conti, F. Ferrua, F. Pozzo Giuffrida, F. Dionisio, P. Rovere-Querini, S. Marktel, A. Assanelli, S. Piemontese, I. Brigida, M. Zoccolillo, E. Cirillo, G. Giardino, M. G. Danieli, F. Specchia, L. Pacillo, S. Di Cesare, C. Giancotta, F. Romano, A. Matarese, A. A. Chetta, M. Trimarchi, A. Laurenzi, M. De Pellegrin, S. Darin, D. Montin, M. Marinoni, R. M. Dellepiane, V. Sordi, V. Lougaris, A. Vacca, R. Melzi, R. Nano, C. Azzari, L. Bongiovanni, C. Pignata, C. Cancrini, A. Plebani, L. Piemonti, C. Petrovas, R. Di Micco, M. Ponzoni, A. Aiuti, M. P. Cicalese, G. Fousteri, Follicular helper T cell signature of replicative exhaustion, apoptosis, and senescence in common variable immunodeficiency. *Eur. J. Immunol.* **52**, 1171–1189 (2022).
43. L. Llao-Cid, P. M. Roessner, V. Chapaprieta, S. Ozturk, T. Roider, M. Bordas, A. Izcue, D. Colomer, S. Dietrich, S. Stilgenbauer, B. Hanna, J. I. Martin-Subero, M. Seiffert, EOMES is essential for antitumor activity of $CD8^+$ T cells in chronic lymphocytic leukemia. *Leukemia* **35**, 3152–3162 (2021).
44. Y. Wolf, A. C. Anderson, V. K. Kuchroo, TIM3 comes of age as an inhibitory receptor. *Nat. Rev. Immunol.* **20**, 173–185 (2020).
45. X. Liu, D. F. Hoft, G. Peng, Senescent T cells within suppressive tumor microenvironments: Emerging target for tumor immunotherapy. *J. Clin. Invest.* **130**, 1073–1083 (2020).
46. M. Mittelbrunn, G. Kroemer, Hallmarks of T cell aging. *Nat. Immunol.* **22**, 687–698 (2021).
47. G. Hodge, S. Hodge, P. N. Reynolds, M. Holmes, Airway infection in stable lung transplant patients is associated with decreased intracellular T-helper type 1 pro-inflammatory cytokines in bronchoalveolar lavage T-cell subsets. *Transplant Infect. Dis.* **10**, 99–105 (2008).
48. G. Hodge, S. Hodge, D. Chambers, P. N. Reynolds, M. Holmes, Acute lung transplant rejection is associated with localized increase in T-cell IFNγ and TNFα proinflammatory cytokines in the airways. *Transplantation* **84**, 1452–1458 (2007).
49. G. Hodge, S. Hodge, P. N. Reynolds, M. Holmes, Compartmentalization of intracellular proinflammatory cytokines in bronchial intraepithelial T cells of stable lung transplant patients. *Clin. Exp. Immunol.* **145**, 413–419 (2006).
50. G. Hodge, S. Hodge, P. N. Reynolds, M. Holmes, Increased intracellular pro- and anti-inflammatory cytokines in bronchoalveolar lavage T cells of stable lung transplant patients. *Transplantation* **80**, 1040–1045 (2005).
51. D. Focosi, M. Bestagno, O. Burrone, M. Petrini, $CD57^+$ T lymphocytes and functional immune deficiency. *J. Leukoc. Biol.* **87**, 107–116 (2010).
52. B. I. Shaw, J. R. Espinosa, L. Stempora, A. Miller, B. Adams, A. D. Kirk, Functional characteristics and phenotypic plasticity of $CD57^+PD1^-$ CD4 T cells and their relationship with transplant immunosuppression. *J. Immunol.* **206**, 1668–1676 (2021).
53. H. Sun, C. R. Hartigan, C.-W. Chen, Y. Sun, M. Tariq, J. M. Robertson, S. M. Krummey, A. K. Mehta, M. L. Ford, TIGIT regulates apoptosis of risky memory T cell subsets implicated in belatacept-resistant rejection. *Am. J. Transplant.* **21**, 3256–3267 (2021).
54. J. Espinosa, F. Herr, G. Tharp, S. Bosinger, M. Song, A. B. Farris III, R. George, J. Cheeseman, L. Stempora, R. Townsend, A. Durrbach, A. D. Kirk, $CD57^+$ CD4 T cells underlie belatacept-resistant allograft rejection. *Am. J. Transplant.* **16**, 1102–1112 (2016).

55. O. Brugière, D. Mouren, J. Trichereau, A. Vallee, I. Kuzniak, S. Hirschi, B. Renaud-Picard, M. Reynaud-Gaubert, A. Nieves, V. Bunel, J. Messika, X. Demant, J. Macey, J. Le Pavec, G. Dauriat, C. Saint-Raymond, L. Falque, J. F. Mornex, A. Tissot, A. Foureau, A. L. Borgne Krams, V. Bousseau, A. Magnan, C. Picard, A. Roux, E. Carosella, J. LeMaoult, N. Rouas-Freiss, COLT Consortium, Chronic lung allograft dysfunction is associated with an early increase of circulating cytotoxic CD4+CD57+ILT2+ T cells, selectively inhibited by the immune check-point HLA-G. *J. Heart Lung Transplant.* **41**, 626–640 (2022).
56. F. Hassouneh, D. Goldeck, A. Pera, D. van Heemst, P. E. Slagboom, G. Pawelec, R. Solana, Functional changes of T-cell subsets with age and CMV infection. *Int. J. Mol. Sci.* **22**, 9973 (2021).
57. V. Libri, R. I. Azevedo, S. E. Jackson, D. Di Mitri, R. Lachmann, S. Fuhrmann, M. Vukmanovic-Stejic, K. Yong, L. Battistini, F. Kern, M. V. Soares, A. N. Akbar, Cytomegalovirus infection induces the accumulation of short-lived, multifunctional $CD4^+CD45RA^+CD27^-$ T cells: The potential involvement of interleukin-7 in this process. *Immunology* **132**, 326–339 (2011).
58. D. Di Mitri, R. I. Azevedo, S. M. Henson, V. Libri, N. E. Riddell, R. Macaulay, D. Kipling, M. V. Soares, L. Battistini, A. N. Akbar, Reversible senescence in human $CD4^+CD45RA^+CD27^-$ memory T cells. *J. Immunol.* **187**, 2093–2100 (2011).
59. T. Martinu, A. Koutsokera, C. Benden, E. Cantu, D. Chambers, M. Cypel, J. Edelman, A. Emtiazjoo, A. J. Fisher, J. R. Greenland, D. Hayes Jr., D. Hwang, B. C. Keller, E. D. Lease, M. Perch, M. Sato, J. L. Todd, S. Verleden, J. von der Thusen, S. S. Weigt, S. Keshavjee, bronchoalveolar lavage standardization workgroup, International Society for Heart and Lung Transplantation consensus statement for the standardization of bronchoalveolar lavage in lung transplantation. *J. Heart Lung Transplant.* **39**, 1171–1190 (2020).
60. E.-A. D. Amir, K. L. Davis, M. D. Tadmor, E. F. Simonds, J. H. Levine, S. C. Bendall, D. K. Shenfeld, S. Krishnaswamy, G. P. Nolan, D. Pe'er, viSNE enables visualization of high dimensional single-cell data and reveals phenotypic heterogeneity of leukemia. *Nat. Biotechnol.* **31**, 545–552 (2013).
61. Y. Benjamini, D. Yekutieli, The control of the false discovery rate in multiple testing under dependency. *Ann. Statistics* **29**, 1165–1188 (2001).
62. G. X. Y. Zheng, J. M. Terry, P. Belgrader, P. Ryvkin, Z. W. Bent, R. Wilson, S. B. Ziraldo, T. D. Wheeler, G. P. McDermott, J. Zhu, M. T. Gregory, J. Shuga, L. Montesclaros, J. G. Underwood, D. A. Masquelier, S. Y. Nishimura, M. Schnall-Levin, P. W. Wyatt, C. M. Hindson, R. Bharadwaj, A. Wong, K. D. Ness, L. W. Beppu, H. J. Deeg, C. McFarland, K. R. Loeb, W. J. Valente, N. G. Ericson, E. A. Stevens, J. P. Radich, T. S. Mikkelsen, B. J. Hindson, J. H. Bielas, Massively parallel digital transcriptional profiling of single cells. *Nat. Commun.* **8**, 14049 (2017).
63. A. Butler, P. Hoffman, P. Smibert, E. Papalexi, R. Satija, Integrating single-cell transcriptomic data across different conditions, technologies, and species. *Nat. Biotechnol.* **36**, 411–420 (2018).
64. C. Hafemeister, R. Satija, Normalization and variance stabilization of single-cell RNA-seq data using regularized negative binomial regression. *Genome Biol.* **20**, 296 (2019).
65. H. Spencer, D. Rampling, P. Aurora, D. Bonnet, S. L. Hart, A. Jaffe, Transbronchial biopsies provide longitudinal evidence for epithelial chimerism in children following sex mismatched lung transplantation. *Thorax* **60**, 60–62 (2005).
66. G. La Manno, R. Soldatov, A. Zeisel, E. Braun, H. Hochgerner, V. Petukhov, K. Lidschreiber, M. E. Kastriti, P. Lönnerberg, A. Furlan, J. Fan, L. E. Borm, Z. Liu, D. van Bruggen, J. Guo, X. He, R. Barker, E. Sundström, G. Castelo-Branco, P. Cramer, I. Adameyko, S. Linnarsson, P. V. Kharchenko, RNA velocity of single cells. *Nature* **560**, 494–498 (2018).
67. V. Bergen, M. Lange, S. Peidli, F. A. Wolf, F. J. Theis, Generalizing RNA velocity to transient cell states through dynamical modeling. *Nat. Biotechnol.* **38**, 1408–1414 (2020).
68. G. Katz, A. L. Snow, Fluorescence-activated cell sorting-based quantitation of T cell receptor restimulation-induced cell death in activated, primary human T cells. *Methods Mol. Biol.* **979**, 15–23 (2013).
69. G. M. Verleden, A. R. Glanville, E. D. Lease, A. J. Fisher, F. Calabrese, P. A. Corris, C. R. Ensor, J. Gottlieb, R. R. Hachem, V. Lama, T. Martinu, D. A. H. Neil, L. G. Singer, G. Snell, R. Vos, Chronic lung allograft dysfunction: Definition, diagnostic criteria, and approaches to treatment—A consensus report from the Pulmonary Council of the ISHLT. *J. Heart Lung Transplant.* **38**, 493–503 (2019).

Acknowledgments: We wish to thank M. Oberle, M. Cuesta, I. Avramov, and other members of the Toronto Lung Transplant Program Biobank for assistance with sample procurement and storage. We thank R. Ghany for management of the Toronto Lung Transplant Program Database and R. Zamel for randomization of the discovery and validation groups. We also thank C. Guidos and D. Davani for critical input on the design of CyTOF experiments. We also wish to thank S. Crome and S. Colpitts for assistance and advice in planning CITE-seq experiments. **Funding:** This work was funded by Cystic Fibrosis Foundation grants JUVET18AB0 and JUVET23G0 (to S.J.) and MARTIN18I0 (to T.M. and S.J.) by an International Society for Heart and Lung Transplantation Norman Shumway Career Development Award (to S.J.), by a Canadian Society of Transplantation Research Training Award (to S.M.), and by the Caron Thorburn Institute and the University Health Network Foundation. **Author contributions:** S.M.: Writing—original draft, conceptualization, investigation, writing—review and editing, methodology, resources, funding acquisition, data curation, validation, supervision, formal analysis, software, and visualization. L.L.: Conceptualization, investigation, writing—review and editing, and methodology. S.S.: Investigation, writing—review and editing, and data curation. S.Ka.: Investigation. G.W.: Conceptualization, methodology, software, and visualization. B.R.-P.: Conceptualization, writing—review and editing and validation. G.M.: Writing—review and editing, data curation, validation, and formal analysis. R.R.: Investigation, writing—review and editing, methodology, data curation, formal analysis, and visualization. J.O.: Investigation. T.W.: Investigation and methodology. K.F.B.: Investigation, writing—review and editing, formal analysis, and visualization. B.J.: Conceptualization, methodology, investigation, and writing—review and editing. Q.L.: Writing—review and editing, methodology, formal analysis, and software. E.H.: Conceptualization, writing—review and editing, methodology, and formal analysis. M.C.: Investigation, methodology, resources, and validation. D.H.: Conceptualization, methodology, resources, and supervision. J.Y.: Writing—review and editing, methodology, and formal analysis. S.Ke.: Conceptualization, writing—review and editing, methodology, resources, funding acquisition, supervision, formal analysis, and project administration. T.M.: Conceptualization, investigation, writing—review and editing, methodology, funding acquisition, supervision, and visualization. S.J.: Writing—original draft, conceptualization, investigation, writing—review and editing, methodology, resources, funding acquisition, data curation, validation, supervision, formal analysis, project administration, and visualization. **Competing interests:** S.M., S.Ke., and S.J. have filed US patent application number US63/460,274 (pending, filed 18 April 2023 with the US Patent and Trademark Office) on in relation to the work in this manuscript. The authors declare that they have no other competing interests. **Data and materials availability:** The CyTOF raw data and CITE-seq Seurat object for this study have been deposited in https://zenodo.org/records/14538146. All data needed to evaluate the conclusions in the paper are present in the paper and/or the Supplementary Materials.

Submitted 17 April 2024
Accepted 14 February 2025
Published 21 March 2025
10.1126/sciadv.adp9052